TWO-LAYER EXCHANGE FLOW THROUGH A CONTRACTION WITH FRICTIONAL EFFECTS

By

EMILY ANNE CHEUNG

B.Sc., The University of British Columbia, 1988

A THESIS SUBMITTED IN PARTIAL FULFILLMENT OF
THE REQUIREMENTS FOR THE DEGREE OF
MASTERS OF APPLIED SCIENCE

in

THE FACULTY OF GRADUATE STUDIES

(Civil Engineering)

We accept this thesis as conforming
to the required standard

THE UNIVERSITY OF BRITISH COLUMBIA

September 1990

In presenting this thesis in partial fulfilment of the requirements for an advanced degree at the University of British Columbia, I agree that the Library shall make it freely available for reference and study. I further agree that permission for extensive copying of this thesis for scholarly purposes may be granted by the head of my department or by his or her representatives. It is understood that copying or publication of this thesis for financial gain shall not be allowed without my written permission.

Department of CIVIL ENGINEERING

The University of British Columbia
Vancouver, Canada

Date Oct 11, 1990

DE-6 (2/88)

Abstract

The gravitational exchange of two fluids of different density through a convergent-divergent contraction is considered. Two-layer exchange flow theory is extended to include frictional effects with an emphasis on the interfacial friction. The magnitude of the interfacial friction is found to be greater than previously suggested and may be vital to the analysis of exchange flows.

Experiments modelling gravitational exchange flow through a convergent-divergent contraction were conducted in the hydraulics laboratory at the University of British Columbia to test the hydraulic solutions that have been developed on two-layer exchange flow. A comparison of the theoretical solutions and experimental results is made. Experiments conducted provide data for evaluating the theoretical findings and help in locating the hydraulic controls of the experiment along with quantifying the magnitude of interfacial friction coefficient. A comparison is made between numerous values obtained for the interfacial friction coefficients by previous investigators and the experimental results of the present study. Flow visualization is used to study the Kelvin-Helmholtz and Holmboe instabilities that form at the interface of the two layers.

Table of Contents

List of Tables

List of Figures

List of Figures (continued)

List of Symbols

A_j	cross sectional area of layer j
$b(x)$	width of flow
b_o	width of flow at throat
d	relative displacement of velocity and density profile interfaces
E	mechanical energy per unit volume for single layer flow
E_j	mechanical energy per unit volume for layer j (Eq. 4.1 and 4.2)
EI	internal energy for two-layer flow (Eq. 4.3)
f	Darcy coefficient
F_Δ^2	stability Froude number (Eq. 3.11)
Fr or F	Froude number (Eq. 3.4)
F_E^2	external Froude number
F_I^2	internal Froude number (Eq. 3.10)
f_I	interfacial friction coefficient
f_w	wall friction coefficient
f_s	surface friction coefficient
h	density interface thickness
$h_s(x)$	height of bottom variations in topography
g	gravitational acceleration
$g'=\varepsilon g$	modified gravitational acceleration
G^2	composite Froude number (Eq. 3.6)
J	bulk Richardson number
n	number of layers
P	wetted perimeter

List of Symbols (continued)

q	volumetric flow rate per unit width
Q	volumetric flow rate
$r=\rho_1/\rho_2$	density ratio
Re	Reynolds number
Rh	hydraulic radius
Ri	gradient Richardson number
S	surface area
S_f	friction slope (Eq. 4.18)
S_o	topographical slope (Eq. 4.21)
t	time
u	critical velocity (Eq. 6.2)
u_j	horizontal component of velocity for layer j
x	horizontal direction
y	total depth of flow
y_j	depth of flow for layer j
y_2'	nondimensional interface height (Eq. 6.1)

List of Symbols (continued)

Greek	
α	ratio of interfacial friction to wall friction
$\alpha=kh$, §8.2	instability wave number
β	ratio of surface friciton to wall friction
δ	mixing layer thickness
$\delta'_{max} = \delta/y$	dimensionless maximum interface thickness
$\varepsilon=(\rho_2-\rho_1)/\rho_2$	relative density difference
λ	wavelength
π	mathematical constant, 3.14
ρ_j	density of layer j
ψ	friction parameter (Kaneko)
τ	shear stress

Acknowledgements

Many thanks to Dr. Gregory A. Lawrence who has given me endless hours of support and encouragement. His advice and suggestions on the work were invaluable to the completion of this project. Without his support and patience, this work would not have been possible. I would also like to thank my husband, Bill, for all his moral support during the two years of my masters program and his comments on numerous drafts of my thesis.

This work is dedicated to my son, Benjamin, who for the first seven months of his life shared his mother with this thesis project.

1. INTRODUCTION

Density stratifications due to temperature and/or salinity variations occur naturally around the world in bodies of water and the atmosphere. The exchange of two fluids of different density often occurs when two bodies of water are connected by a strait or channel. In the past forty years, the interest in exchange flows in many fields of study including oceanography, the atmospheric sciences, hydraulics and environmental engineering has grown considerably.

A prime example that has attracted perhaps the greatest interest is the Strait of Gibraltar where the more saline Mediterranean Sea exchanges water with the Atlantic Ocean via the Strait. This is due to the high evaporation rate that exceeds the precipitation in the Mediterranean. Other Straits in which important exchange flow occur are discussed in Defant (1961). They include the Strait of Bab el Mandeb which connects the Indian Ocean with the highly saline Red Sea, and the Strait of Hormuz which connects the Arabian Sea and the Persian Gulf. Excess run-off flowing into the ocean through a connecting Strait in more humid regions also cause exchange flows. For example, the Black Sea is joined by the Bosporus to the Sea of Marmara which in turn is connected by the Dardanelles with the Mediterranean. As well, Cabot Strait lies between the Gulf of St. Lawrence and the Atlantic Ocean.

Other waterways that experience flows that may be

stratified due to density differences include fjords, lakes, reservoirs, locks and estuaries. However in some of these situations the flow may not necessarily be exchanging as in the case of arrested salt wedges in fjords and estuaries where the lower layer of fluid is stagnant for long periods of time. In the Strait of Georgia and Knight Inlet along the coast of British Columbia, stratified flows are found during times of large river discharge (Thomson, 1981).

Interfacial mixing between the layers of stratified flows has created concern in many areas where pollution or salinity threaten the quality of water. For example, an exchange flow occurs in the ship canal connecting Lake Ontario with the heavily polluted Hamilton Harbour. An understanding of this exchange flow is crucial to the evaluation of potential measures to improve water quality in Hamilton Harbour, see Hamblin and Lawrence (1990).

The environmental effects caused by the construction of a bridge and tunnel system for the Great Belt Link in Denmark that is proposed to span the Great Belt, a main artery for exchange flow to the Baltic Sea, are to be minimized (Hansen and Moeller 1990). The government of Denmark has decreed that the exchange flow shall remain the same after the construction of the link; therefore, the added resistance of the tunnel and bridge piers must be compensated such that exchange to the Baltic remains unchanged.

The shear produced at the interface of stratified flows has

also attracted the interest of numerous authors (e.g. Koop and Browand 1979 and Thorpe 1987). The generation of turbulence and mixing in stratified flows is a function of the stability of the sheared density interface. Understanding the processes involved in the shear and mixing is pertinent to the advance of the study of exchange flows. The shear between the stratified layers generates instabilities known as Kelvin-Helmholtz and Holmboe instabilities. The magnitude of this shear and the size of the Kelvin-Helmholtz billows can be predicted from internal hydraulic theory; however, good agreement between observations and predictions has not as yet been obtained.

An interfacial friction coefficient is used to quantify the shear that is produced at the interface of two flows. Although there seems to be no consensus on a method of quantifying this coefficient, various authors have examined this problem and further research is included in the present study.

1.1 Objectives

There are three primary objectives of this study:

1. To test experimentally the existing hydraulic solutions for exchange flow through a contraction.
2. To obtain good flow visualization of the exchange flow in experimental conditions.
3. To extend the theory of exchange flows to include frictional effects and locate the internal hydraulic controls.

A review of the history of exchange flows is presented in §2 including two-layer flow, mixing and friction coefficients. The internal hydraulic theory is reviewed in §3 covering assumptions, equations of motion, Froude numbers and a discussion of interfacial instabilities. The theoretical development of exchange flow is covered in §4 with application to exchange flow through a convergent-divergent contraction presenting formulation with frictional considerations. Details of the experimental work are provided in §5 followed by a description of the solution technique and the evaluation of the friction coefficients in §6. A discussion on the interfacial friction follows in §7 with the results and conclusions given in §8 and §9. Finally, further recommendations for additional research are discussed in §10.

2. LITERATURE REVIEW

2.1 Hydraulics of Two-layer Flow

Among the first theoretical analyses of two-layer flow were those of Schijf and Schönfeld (1953) and Stommel and Farmer (1953). They examined numerous examples including salt wedges, salt intrusion in estuaries and lock exchange flow. The analysis of Schijf and Schönfeld (1953) includes frictional effects in the formulation of two-layer flow equations, but assumes negligible surface shear and side wall shear stresses. They have also expanded the theory to lock exchange flow, salt wedges and salt intrusion in an estuary, but focus primarily on turbulence and other diffusion mechanisms.

Subsequently, Wood (1968, 1970) also examined lock exchange flow and the identification of points of internal hydraulic control. Wood (1968) identifies two points of control for stratified flows through a contraction: one at the point of minimum width and the other called the point of virtual control. Both control points can be located again by satisfying the condition of the composite Froude number, $G^2=1$. Wood (1970) also looks at lock exchange flow but does not deal with friction.

Lawrence (1985) presents additional work on two-layer flow with an emphasis on flow over an obstacle. A classification scheme was developed to identify regimes of steady two-layer flow and the location of internal hydraulic controls.

Denton (1987) looks at locating and identifying hydraulic

controls and analyzes single layer flow including frictional effects and two-layer flow assuming negligible friction by internal energy methods. Recently, Denton (1990) extended the work to unidirectional three-layer flow over a hump and through a contraction and classifies different flow regimes, each with a different set of locations for internal hydraulic control.

2.2 Exchange Flow

Exchange flow through a long strait was examined by Assaf and Hecht (1974) whereby the flow is bounded by controls at either end of the strait. Their analysis models an enclosed basin by balancing friction, salt and mass through the strait. Results of the model are compared with observations made of the Strait of Gibraltar, the Bosphorus and the Bab el Mandeb Strait.

Papers by Armi (1986), Armi and Farmer (1986) and Farmer and Armi (1986) have presented internal hydraulic theory on exchange flows. In particular, gravitational exchange flow of two fluids of slightly different density through a contraction has been examined by Armi and Farmer (1986). Armi and Farmer (1986) examine maximal two-layer exchange flow through a contraction with barotropic flow, that is $q_1 \neq q_2$, where q is the volumetric flow rate, and also acknowledge the presence of the two control points, the narrowest section (throat) and the virtual control, separated by a region of subcritical flow. In the absence of any barotropic component or any frictional effects, these two control points coalesce.

Farmer and Armi (1986) have presented detailed exchange flow analysis for both flow over a sill and the combination of a sill and a contraction with application of the hydraulics of layered flows to field measurements of the Strait of Gibraltar. A considerable amount of field work and application of exchange flow theory was done by Armi and Farmer (1988) in the Strait of Gibraltar and recently applied to a model of the Strait.

2.3 Stability and Mixing

At the interface of two statically stable fluids is a horizontal shear which may generate instabilities that cause mixing between the two layers. This process has been examined by many authors including Taylor (1931), Goldstein (1931), Turner (1973), Sherman, Imberger & Corcos (1978) and Thorpe (1987). Koop and Browand (1979) studied some of the characteristics of turbulence in stratified fluids with emphasis on conditions which may approximate those found in oceans. They also suggest an upper bound of turbulent mixing and conclude that the Richardson number, Reynolds number and Schmidt number all become important in the analysis of turbulence.

Lawrence (1985) presents work on two-layer flow with an emphasis on flow over an obstacle. He examines internal hydraulic controls in the flow as it approaches an obstacle and also investigates the dynamics of mixing of the two layers. The extent to which mixing occurs was examined by Lawrence (1989) and he poses the question, "Can mixing in exchange flows be

predicted using internal hydraulics?". Lawrence states that an upper bound on the extent of mixing can be predicted from the internal hydraulics.

A detailed examination of the stability Froude number, F_Δ^2, was done recently by Lawrence (1990a) and he notes that it is of great significance in the prediction of mixing in two-layer flows. Lawrence, Browand & Redekopp (1990) discuss the stability of a sheared interface stating that it is fundamental to the generation of mixing in stratified flows and is dependent on the velocity and density differences of the flowing layers of fluid. Their theoretical and experimental results are presented covering a more general study of interfacial instabilities and presented are stability diagrams used in the prediction of wavelengths of both the Kelvin-Helmholtz and Holmboe modes of instability. The shear at the interface leads to the formation of Kelvin-Helmholtz and Holmboe instabilities which are also discussed by Thorpe (1987).

2.4 Friction Coefficients

The dynamics of frictional exchange flows involves an examination of the shear stresses on the walls and interface of stratified flows which are mainly dependent on two coefficients of friction namely the wall friction coefficient, f_w, and the interfacial friction coefficient, f_I. Although evaluation of the wall friction coefficient has been well documented (Henderson 1966), there has proven to be great difficulties in evaluating

the interfacial friction coefficient. Often an order of magnitude estimate of, 10^{-3}, is used to quantify the coefficient. Although methods of defining the interfacial friction coefficient were presented as early as 1953 by Schijf and Schönfeld, there has been no conclusion as to which method is most appropriate or if any of the presented methods are adequate for calculating the coefficient. A detailed review and discussion of various authors' methods of determining the interfacial friction coefficient are presented in §7 after some of the pertinent theory has been discussed.

3. REVIEW OF HYDRAULIC THEORY

3.1 Basic Assumptions

The focus of this analysis of layered flows is based on the assumptions of steady two-dimensional, non-rotating, inviscid flow. The assumption is also made that there is negligible free surface deflection. There is assumed to be no external forcing, for example, tidally driven flows, such that the exchange flow is due to the density differences in the two layers. The analysis focuses primarily on two-layer flows; however, extension to any number of layers has been formulated by others including Benton (1954), Baines (1988), and Denton (1990). It is useful here to begin by understanding the hydraulics of single layer flow before expanding to two-layer flow. Armi (1986) and Lawrence (1989) discuss the basic hydraulic theory involved in two-layer flow; however, a review of some of the pertinent theory follows in the next section.

3.2 Equations of Motion

Assuming steady flow, the motion of layered flows is governed by

$$\frac{1}{\rho_j}\frac{\partial E_j}{\partial x}=0 \qquad (3.1)$$

and the continuity equation

$$\frac{1}{b}\frac{\partial Q_j}{\partial x}=0 \qquad (3.2)$$

where j is the number of layers (j=1 for single layer flow), ρ_j is the density of layer j, b is the width of the flow, Q_j is the volumetric flow rate and E_j is the mechanical energy per unit volume defined as

$$E_j = (p+\rho_j g y_j) + \frac{1}{2}\rho_j u_j^2 \qquad (j = 1,n) \qquad (3.3)$$

where p is the pressure, assumed hydrostatic, g is the acceleration due to gravity, y_j and u_j are the depth and the velocity of layer j and n is the number of layers considered. Although Equations 3.1 and 3.2 are one-dimensional, they can be applied to flow through a contraction provided the contraction is gentle.

3.3 Review of Froude Numbers

Hydraulic flow is traditionally classified by the nondimensional Froude number that is best introduced as a ratio of convective velocity to phase speed. In single layer flow, a flow is classified as subcritical where the Froude number of the flow is less than 1; supercritical where the Froude number is greater than 1; and the control point of the flow is located where the Froude number has a value of 1. The control point is

a transition point and provides a starting point required to study flows. Henderson (1966) gives a general definition of a hydraulic control as a point at which there is a known depth-discharge relationship. An example of a control can be seen at a sluice gate at which upstream flow is subcritical and downstream flow is supercritical; here, the sluice gate acts as a control device (Henderson, 1966). The Froude number is evaluated by

$$Fr^2 = \frac{u^2}{gy} \tag{3.4}$$

This theory can easily be expanded to two-layer flow where the densimetric Froude number for each layer simply becomes

$$Fr_j^2 = \frac{u_j^2}{g'y_j} \tag{3.5}$$

where g' is the modified acceleration due to gravity; that is, $g' = \varepsilon g$ and ε is defined by $\varepsilon = (\rho_2-\rho_1)/\rho_2$. However, in two-layer flow it is important to recognize a composite Froude number denoted G^2 and defined by Equation 3.6.

$$G^2 = Fr_1^2 + Fr_2^2 - \varepsilon Fr_1^2 Fr_2^2 \tag{3.6}$$

In this case the singularity condition or control occurs where the composite Froude number, $G^2=1$ analogous to $Fr^2=1$ in single layer flow. Typically the Boussinesq approximation is made that

$\varepsilon \ll 1$ (of order 10^{-3}) such that G^2 is approximated by

$$G^2 = Fr_1^2 + Fr_2^2 \qquad (3.7)$$

The location of the control point in a convergent-divergent channel for inviscid flows is historically the narrowest point or throat of the channel (Armi and Farmer, 1986). Variation of the Froude numbers through a contraction is best diagrammed on the Froude number plane as shown by Armi and Farmer (1986). The flow is critical at the throat ($G^2=1$) and on either side of the control point or throat is supercritical flow ($G^2>1$).

In conjunction with G^2, three additional Froude numbers, F_I^2, F_E^2, and F_Δ^2; the internal, external and stability Froude numbers respectively, become important in two-layer flow. Recall that the Froude number is defined as the ratio of convective velocity to the phase speed. This is also applicable to the internal and external Froude numbers. The celerity or characteristic velocity of long waves both on the surface (external) and along the interface of two-layer flow (internal) is a sum of a convective velocity and a phase speed. Note that although the composite Froude number may determine the criticality of two-layer flow, it cannot be defined as the single layer Froude number as it is not a ratio of convective velocity to phase speed for both internal and external waves (Lawrence 1990a).

Perhaps the most useful of these three Froude numbers is

the stability Froude number. It can be regarded as the inverse of a bulk Richardson number and is used in quantifying the mixing layer thickness, the stability of the flow and its susceptibility to instabilities at the interface. A fundamental relationship (Lawrence 1985, 1990a) exists between these four Froude numbers given by:

$$(1-G^2) = (1-F_\Delta^2)(1-F_E^2)(1-F_I^2) \qquad (3.8)$$

However, for exchange flow through a contraction, $F_E^2 \approx 0$ from the assumption of negligible free surface deflection. Therefore the relationship between the Froude numbers, Equation 3.8 is reduced to the following.

$$(1-G^2) = (1-F_\Delta^2)(1-F_I^2) \qquad (3.9)$$

Variation of these three Froude numbers along the contraction for inviscid flows is better understood by the illustration shown in Figure 1. Note that the location of the control is the point at which $G^2=1$. For Boussinesq two-layer flows the external Froude number is the same as the single layer Froude number (3.4). The internal Froude number (Lawrence 1985, 1990a) is defined

$$F_I = \frac{u_1 y_2 + u_2 y_1}{\sqrt{g' y \, y_1 y_2 (1-F_\Delta^2)}} \qquad (3.10)$$

where $y = y_1+y_2$. The significance of the stability Froude number is discussed further in the following section.

3.4 The Stability Froude Number

The interfacial long wave stability Froude number is a representation of the strength of the velocity shear across the interface of the two fluid layers. This stability Froude number is defined as:

$$F_{\Delta}^2 \equiv \frac{\Delta u^2}{g'y} \qquad (3.11)$$

where $\Delta u = u_1 - u_2$ and y is the total depth of flow. If frictional effects are ignored, Lawrence (1990b) has shown that $F_{\Delta}^2=1$ throughout the channel if the flow rate ratio, $q_r=1$. However, taking into account the frictional effects reduces F_{Δ}^2 proportionally as the flow rates in each layer are actually less than the theoretical ideal values.

Lawrence (1990a) notes from Equation 3.10, Long's stability criterion for long internal waves, $F_{\Delta}^2 \leq 1$, must be satisfied in order for the internal Froude number to have real values. Long's stability criterion applies only to long internal waves, since the assumption of a hydrostatic pressure distribution precludes the existence of short waves. To quote Long (1956), 'If we abandon the hydrostatic assumption momentarily, we find that sufficiently short infinitesimal waves are unstable for any shear.' Thorpe (1987) notes that the interface is unstable to instabilities even for $F_{\Delta}^2 \ll 1$ including the Kelvin-Helmholtz and Holmboe instabilities. Note that the higher F_{Δ}^2 the larger the instabilities.

3.5 Interfacial Instabilities

3.5.1 Kelvin-Helmholtz Instabilities

The Kelvin-Helmholtz instabilities at the interface of the two fluids cause considerable mixing to occur. Turner (1973) states, "When a sufficiently large shear is applied across a density interface and is such that the gradient Richardson number falls below a critical value of about 0.25, Kelvin-Helmholtz waves will grow and overturn to produce patches of turbulent mixing." Where the gradient Richardson number is defined, $Ri=N^2/(\partial u/\partial z)^2$, and the buoyancy frequency, $N^2=(g/\rho)(d\rho/dz)$. This mechanism of mixing causes the production of interfacial layers in stratified fluids. Wilkinson and Wood (1983) describe the Kelvin-Helmholtz instability as one which converts kinetic energy of large-scale shear flows to smaller dissipative scales.

These three-dimensional disturbances effectively mix most of the fluid that is entrained by the Kelvin-Helmholtz billows. As a result, maximum interface thickness, δ_{max}, can be predicted. Lawrence (1990b) presents a diagram showing the relationship of δ_{max} and F_Δ^2 for the case of $F_\Delta^2=O(1)$ which is the situation considered here. Further consideration of this diagram is made in §8.1.

Velocity and density profiles are modelled using the piecewise linear approximations shown in Figure 2. Two layers are shown of different densities with a density interface thickness of h. The shear at the interface of the two flows

leads to the formation of Kelvin-Helmholtz and Holmboe type instabilities.

3.5.2 Holmboe Instabilities

The Holmboe instability was first studied by Holmboe (1962) and more recently by Browand and Winant (1973), Koop and Browand (1979), Smyth, Klaassen and Peltier (1988) and Lawrence, Browand & Redekopp (1990). Although the occurrence of Kelvin-Helmholtz instabilities have been well documented, there is little documented evidence of Holmboe instabilities. The Holmboe mode of instability is known to dominate only in the case where the velocity and density interfaces are not displaced vertically with respect to each other. Linear stability theory predicts the formation of the Holmboe instability when the gradient Richardson number exceeds a critical value of approximately 0.25 (For further discussion see Smyth et al, 1988 and 1989).

These instabilities are depicted by a series of sharply cusped crests which protrude into each layer of fluid. Portions of the top of the cusps are occasionally torn away and become mixed with the layers of fluid flowing by. More fluid is drawn up by these cusps as the Richardson number approaches zero ultimately forming Kelvin-Helmholtz billows.

4. THEORETICAL DEVELOPMENT

4.1 Energy and Shear Stress

Consider the Mechanical Energy per unit volume for each layer separately.

$$E_1 = \rho_1 g y + \frac{1}{2}\rho_1 u_1^2 \tag{4.1}$$

$$E_2 = \rho_1 g y + (\rho_2 - \rho_1) g y_2 + \frac{1}{2}\rho_2 u_2^2 \tag{4.2}$$

Subtracting Equation 4.1 from 4.2 and dividing by the unit weight of the lower layer, $\rho_2 g'$, gives us an equation for the internal energy head. For two-layer flow, the internal head is obtained from

$$EI = y_2 + \frac{1}{2g'}(u_2^2 - u_1^2) \tag{4.3}$$

similar to that of the total energy or Bernoulli equation for single layer flow given by Equation 4.4.

$$E = y + \frac{u^2}{2g} \tag{4.4}$$

Differentiating Equations 4.1 and 4.2, the result is two simultaneous equations which when solved produce an equation for the slope of the interface. Denton shows these equations neglecting frictional effects. Schijf and Schönfeld include the

bottom and interfacial shear stresses and assume negligible side wall and surface shear stresses. They also state that their formulas are approximate, based on the assumption that $\varepsilon \ll 1$.

In this section the theory is expanded to evaluate frictional effects caused by the surface, the side walls, the interface and the bottom surface. Energy losses due to friction are denoted by the shear stresses at the four surfaces respectively and can be represented by the following equations.

$$\textit{Surface} \qquad \tau_s = -f_s \rho_1 u_1 |u_1| \tag{4.5}$$

$$\textit{Walls} \qquad \tau_w = -f_w \rho_j u_j |u_j| \tag{4.6}$$

$$\textit{Upper layer Interface} \qquad \tau_{I1} = -f_I \overline{\rho} (\Delta u)^2$$

$$\textit{Lower layer Interface} \qquad \tau_{I2} = f_I \overline{\rho} (\Delta u)^2 \tag{4.8}$$

$$\textit{Bottom} \qquad \tau_b = -f_w \rho_2 u_2 |u_2| \tag{4.9}$$

For Boussinesq flows, $\overline{\rho}$ is estimated as ρ_1 for the upper layer and ρ_2 for the lower layer. The convention has been adopted that the positive direction of flow is that of the upper layer such that $|u_1| = u_1$ and $|u_2| = -u_2$. The shear stresses are defined diagrammatically in Figure 3 by a sketch of an element of fluid from each layer. Introduced in the shear stress equations are the friction coefficients where f_s is the surface friction coefficient, f_w is the wall friction coefficient and f_I is the interfacial friction coefficient. Note that throughout the

analysis $f_w=f/8$; so that conventionally f, the Darcy coefficient, is equivalent to $8f_w$. Note that f_I does not acquire the same value as f_w nor f_s since the Darcy coefficient would be different for the interface, the surface and the walls. Such formulations for the interfacial shear and bottom shear are similar to those presented by Schijf and Schönfeld (1953). We assume that the energy losses are due to these shear stresses on all the walls, the surface and at the interface of the two flows such that

$$\frac{dE_j}{dx} = \frac{\sum \tau_j \, dS}{A_j \, dx} \tag{4.10}$$

where S is the surface area and A_j is the cross sectional area. The left side of Equation 4.9 is evaluated by differentiating (4.1) and (4.2) for each layer respectively. The right side of (4.10) for each layer are evaluated by

$$\frac{\sum \tau_1 dS}{A_1 dx} = -f_w \rho_1 u_1^2 \frac{2}{b} - f_i \rho_1 \Delta u^2 \frac{1}{y_1} - f_s \rho_1 u_1^2 \frac{1}{y_1} \tag{4.11}$$

$$\frac{\sum \tau_2 dS}{A_2 dx} = f_w \rho_2 u_2^2 \frac{2}{b} + f_i \rho_2 \Delta u^2 \frac{1}{y_2} + f_w \rho_2 u_2^2 \frac{1}{y_2} \tag{4.12}$$

with the shear stresses defined earlier in Equations 4.5 - 4.9.

4.2 Exchange Flow Through a Contraction

The use of the one-dimensional equations (3.1 and 3.2) to multi-layer flows accounting for the shear stresses acting on

the interfacial and boundary surfaces can be reduced to Equation 4.13.

$$\boldsymbol{C}\,\frac{\partial \boldsymbol{v}}{\partial x} = \boldsymbol{D}\,\frac{\partial \boldsymbol{f}}{\partial x} + \boldsymbol{S} \qquad (4.13)$$

For single layer flow

$$\boldsymbol{C} = \begin{bmatrix} u & g \\ y & u \end{bmatrix} \quad \boldsymbol{v} = \begin{bmatrix} u \\ y \end{bmatrix} \quad \boldsymbol{D} = \begin{bmatrix} -g & 0 \\ 0 & Q \end{bmatrix} \quad \boldsymbol{f} = \begin{bmatrix} h_s \\ b^{-1} \end{bmatrix} \quad \boldsymbol{S} = \begin{bmatrix} -f_w u^2 \left(\frac{2}{b} + \frac{1}{y}\right) - f_s u^2 \frac{1}{y} \\ 0 \end{bmatrix}$$

and for two-layer flow

$$\boldsymbol{C} = \begin{bmatrix} u_1 & 0 & g & g \\ 0 & u_2 & rg & g \\ y_1 & 0 & u_1 & 0 \\ 0 & y_2 & 0 & u_2 \end{bmatrix} \quad \boldsymbol{v} = \begin{bmatrix} u_1 \\ u_2 \\ y_1 \\ y_2 \end{bmatrix} \quad \boldsymbol{D} = \begin{bmatrix} -g & 0 \\ -g & 0 \\ 0 & Q_1 \\ 0 & Q_2 \end{bmatrix} \quad \boldsymbol{f} = \begin{bmatrix} h_s \\ b^{-1} \end{bmatrix} \quad \boldsymbol{S} = \begin{bmatrix} -f_w u_1^2 \frac{2}{b} - f_I \Delta u^2 \frac{1}{y_1} - f_s u_1^2 \frac{1}{y_1} \\ f_w u_2^2 \left(\frac{2}{b} + \frac{1}{y_2}\right) + f_I \Delta u^2 \frac{1}{y_2} \\ 0 \\ 0 \end{bmatrix}$$

Generally $h_s(x)$ are the bottom variations in topography, but are not considered in the present study. Note the frictional components appear only in matrix **S** where f_w , f_I and f_s are the wall, interfacial and surface friction coefficients.

Since Equation 4.13 is quasi-linear, the dependent variables $\mathbf{v}_x$ can be expressed as functions of the independent variables $\mathbf{f}_x$. Thus the following four equations are derived.

$$\frac{1}{u_1}\frac{du_1}{dx} = -\left[\frac{1-F_2^2\left(1+{}^{y_2}/_{y_1}\right)}{1-G^2}\right]\frac{1}{b}\frac{db}{dx} - \left[\frac{F_2^2}{1-G^2}\right]\frac{1}{y_1}\frac{dh_s}{dx} + \frac{1}{y_1}\left[\frac{\Delta S_f}{1-G^2}\right] \quad (4.14)$$

$$\frac{1}{u_2}\frac{du_2}{dx} = -\left[\frac{1-F_1^2\left(1+{}^{ry_1}/_{y_2}\right)}{1-G^2}\right]\frac{1}{b}\frac{db}{dx} + \left[\frac{1-F_1^2}{1-G^2}\right]\frac{1}{y_2}\frac{dh_s}{dx} - \frac{1}{y_2}\left[\frac{\Delta S_f}{1-G^2}\right] \quad (4.15)$$

$$\frac{1}{y_1}\frac{dy_1}{dx} = \left[\frac{G^2-F_2^2\left(1+{}^{y_2}/_{y_1}\right)}{1-G^2}\right]\frac{1}{b}\frac{db}{dx} + \left[\frac{F_2^2}{1-G^2}\right]\frac{1}{y_1}\frac{dh_s}{dx} - \frac{1}{y_1}\left[\frac{\Delta S_f}{1-G^2}\right] \quad (4.16)$$

$$\frac{1}{y_2}\frac{dy_2}{dx} = \left[\frac{G^2-F_1^2\left(1+{}^{ry_1}/_{y_2}\right)}{1-G^2}\right]\frac{1}{b}\frac{db}{dx} - \left[\frac{1-F_1^2}{1-G^2}\right]\frac{1}{y_2}\frac{dh_s}{dx} + \frac{1}{y_2}\left[\frac{\Delta S_f}{1-G^2}\right] \quad (4.17)$$

Details of the derivation of Equation 4.17 as an example are given in Appendix A. The friction slope, ΔS_f, which includes the wall, interfacial, bottom, and surface friction, is given by

$$\Delta S_f = \Delta S_{fw} + \Delta S_{fI} + \Delta S_{fb} + \Delta S_{fs}$$

that is

$$\Delta S_f = \frac{2f_w}{b}\left[F_1^2 y_1 + F_2^2 y_2\right] + f_I F_\Delta^2 \frac{Y^2}{y_1 y_2} + f_w F_2^2 + f_s F_1^2 \quad (4.18)$$

where $\Delta S_f = S_{f2} - S_{f1}$ and S_{f1} and S_{f2} are the friction slopes for the upper and lower layers respectively. Note that the density

ratio, $r=\rho_1/\rho_2$ which is also equivalent to $1-\varepsilon$. The Froude number, Fr, is now denoted simply as F.

It is useful here to examine the problem by looking at the internal energy head. The flow within the channel depends on the internal resistance equation from Henderson (1966).

$$\frac{dEI}{dx} = -\Delta S_f \tag{4.19}$$

where S_f can be termed the energy slope or friction slope. Substituting the internal energy head, Equation 4.3, into Equation 4.19, results in an equation for the slope of the interface.

$$\frac{dy_2}{dx} = \frac{S_o - \Delta S_f}{1 - G^2} \tag{4.20}$$

where S_o here is defined as a topographical slope attributable in the present study to the variation of width in the channel and any variation in depth which is considered negligible here. Note that the form of the Equation 4.20 is similar to that derived in Equation 4.17; therefore, expressions for both the topographical slope and the friction slope are determined with the friction slope given by Equation 4.18 and the topographical slope by Equation 4.21.

$$S_o = \left(F_2^2\, y_2 - rF_1^2\, y_1\right) \frac{1}{b} \frac{db}{dx} \tag{4.21}$$

The singular points of Equation 4.20 occur again where the composite Froude number, $G^2=1$. Therefore the control points are found from the numerator of Equation 4.20 where

$$S_o = \Delta S_f \tag{4.22}$$

Two points of control are then identified; one for y_1 and one for y_2 which occur at equal distances on opposite sides of the throat. For each experiment the control points were identified using the above formulation.

5. EXPERIMENTS

5.1 Experimental Apparatus

A two-layer gravitational exchange of salt and fresh water through a convergent-divergent contraction is modelled in a 3.7 x 1.1 x 0.3 m tank. The simplest configuration that incorporates both frictional effects and variable topography was constructed as a first step towards modelling natural configurations. Two reservoirs of approximately 500 litres are joined via a contraction which may be altered in both width and curvature. Both the elevation and plan view of the apparatus are shown in Figure 4.

Each reservoir is independently filled with fluid from the same source by installing a barrier in the throat of the contraction. The density of the right reservoir is increased by dissolving a known quantity of salt as well as fluorescein dye to differentiate between the two flowing layers of fluid.

Initial measurements are taken of the total water depth as well as the channel widths at the throat, channel end points and midway points between the throat and channel ends. These measurements are taken to ensure a width profile similar to the assumed profile (discussed further in §6) since the channel is variable in width along the entire channel length. The modified acceleration due to gravity, g', is calculated knowing the salt content by weight and reservoir volume. Temperature measurements are also taken to attain a value for viscosity

which is required to calculate Reynold's numbers.

The experiment is conducted in a darkened room with two slide projectors mounted on the ceiling above the contraction of the channel. Each projector contains a slide which has mounted on it two razor blades aligned with about only a 1 mm gap to allow for a thin sheet of light (approx. 3 or 4 mm at the water surface) to illuminate a two dimensional view of the flow in the channel. Dissolving fluorescein dye in the more dense layer produces a lower fluorescing "green" layer flowing leftward and a top clear layer or "black" layer flowing right as shown by Figure 5. A photograph of the experimental apparatus in shown in Figure 6.

5.2 Experimental Procedure

After preparation of the two reservoirs and allowing a brief moment for the reservoirs to settle, the barrier at the throat is removed. Due to the density gradient, the fluid in the right reservoir is forced to flow under the less dense fluid setting up an exchange flow. It may take up to a half of a minute before the experiment becomes quasi-steady and the duration is typically approximately 10 minutes enabling sufficient time for measurements and photography to be done.

Polystyrene beads are used as neutrally buoyant particles which are seen when they pass through the thin sheet of light projected through the layers of fluid. Originally these beads are slightly more dense than water (specific gravity of 1.04)

and therefore sink when submersed. However a technique was developed to heat and expand the polystyrene beads so as to make them neutrally buoyant and hence suitable for experimental purposes.

5.3 Velocity Measurements

In order to obtain velocity measurements, long exposures of 3 or 4 seconds are taken in which the polystyrene beads show up clearly as streaks on the photographs. An example photograph, Figure 7, shows the streaks from the beads in both the upper and lower layers. Although this proves worthy for obtaining individual velocities at certain depth locations, it is inadequate for producing velocity profiles throughout the depth of the flow because of insufficient beads passing through the single frame in a particular instance.

To obtain full velocity profiles throughout the depth, a video camera is use to record the experiment in progress. Using an image processor, several images are captured in sequence from the video tape over a known time span and velocities are determined from the relative movement of individual beads throughout the depth of flow. Three examples of the velocity profiles obtained are shown in Figures 8,9, and 10. To validate the assumption of steady flow, a long term analysis of the velocities was done (Figure 11) which shows the startup, a period of quasi-steady flow for approximately 10 minutes and the uncontrolled later portions of the experiment.

6. NUMERICAL ANALYSIS

6.1 The Numerical Model

In order to evaluate the location of the control points and the interfacial friction coefficient, a numerical spreadsheet model was developed using the hydraulic theory discussed in §3 along with §4. The channel profile is assumed to take on the shape represented by $b'=\exp(x')^2$ with b' and x' being nondimensional channel width and length respectively defined by $b'=b/b_o$ and $x'=x/2L$, L is the distance from the throat to the channel ends and b_o is the width at the narrowest point of the channel called the throat. Therefore, the nondimensional channel width can be determined as a function of nondimensional channel length. Choosing an increment interval for the channel length, b' is then determined at each of the increment points along the channel. The height of the interface at each of these points is then evaluated by

$$y_2' = \left\{ \begin{array}{ll} \frac{1}{2}\left(1-\sqrt{1-\frac{1}{b'}}\right) & x<0 \\ \frac{1}{2}\left(1+\sqrt{1-\frac{1}{b'}}\right) & x>0 \end{array} \right\} \qquad (6.1)$$

where y_2' is the nondimensional interface height. This equation is adapted from Lawrence (1990b) assuming that the flow ratio, $q_r=1$ where $q_r = q_1/q_2$ and q is the flow per unit width.

The theoretical velocity at the throat, u, is calculated from Equations 3.5 and 3.7, assuming that $u_1=-u_2$ and $y_1=y_2$ at the throat so that the velocity at the throat, u, for critical flow is evaluated from Equation 6.2.

$$u = \frac{1}{2}\sqrt{g'y} \tag{6.2}$$

However, this results in a theoretical velocity which ignores frictional effects. To compensate, this velocity is reduced to allow for friction by using velocities measured from photographs and analysed from the video tapes of each of the experiments. From the experimental data, a reduction coefficient, k, is determined to factor down the velocity to correspond to the physical values measured such that the theoretical velocity is equal to ku. Profiles taken from numerous experiments at different locations were plotted and a regression curve fit to the data to evaluate the experimental velocities and determine a value of the velocity reduction coefficient. A value of $k = 0.74\pm0.05$, equivalent to 74% of the theoretical velocity was determined to be appropriate. Both the velocities across the channel as well as the variation throughout the depth of the channel are considered in determination of the velocity coefficient.

The flow rate is calculated using the velocity, depth, and width at the throat. Subsequent velocities downstream of the throat are then evaluated using the continuity equation. Froude

numbers for both layers are computed from Equation 3.5. Now all of the required data is available for calculating the composite Froude number which determines the locations of the control points.

To substantiate the assumption that the flow ratio of the two-layers, $q_r = q_1/q_2$, is indeed unity as prescribed for no external forcing, q_r is also evaluated. The stability Froude number (Equation 3.11) evaluated at all locations in the channel proved to be constant for each experiment.

6.2 Evaluation of Friction Coefficients

Due to discrepancies in the literature as to the relative importance of different frictional terms, it is necessary to use the experimental data to look at this problem. All of the friction terms from Equation 4.18 are evaluated to examine the relative magnitude of each. Since all terms are within one order of magnitude, each of the terms are considered significant enough to be included in the analysis.

Values for f_w are calculated from the H. Blasius' solution for a flat plate boundary layer theory (Schlichting 1979) given by

$$f = \frac{2.656}{\sqrt{Re_x}} \tag{6.3}$$

recalling that $f_w = f/8$ and Re_x is the Reynolds number, $Re_x = ux/\nu$, using a length parameter, x, of the length of the

contracted channel. Note that this equation is valid for $Re_x < 5x10^5$ and since the Reynolds number, Re_x, is used, then the wall friction coefficient, f_w, is a function of x. It is also important to realize that the flow is not fully developed thereby the boundary layers do not extend throughout each layer. This is good for examining the interfacial stress since there will be no interference from the wall stresses and the interfacial stress can be determined more accurately.

A constant, β, is introduced to relate the surface friction coefficient to f_w such that $f_s = \beta f_w$. Since a value of β is not determined experimentally, the numerical analysis is done allowing for complete variability of β, $0 \leq \beta \leq 1$. Once f_w is determined from the Blasius equation, the only remaining variable is the interfacial friction coefficient, f_I.

6.3 Control Point Location

Experimental data which include g', b_o, y_o, and u are used in conjunction with the numerical spreadsheet model to determine the location of the control points on either side of the throat which satisfy the singularity condition, $G^2=1$. First G^2 is evaluated everywhere. Then each term of Equation 4.17 is evaluated along the length of the channel to identify the location at which Equation 4.17 is satisfied. In order to evaluate both the friction and topographical slopes, all three friction coefficients are needed. For each of the experiments

conducted the interfacial friction coefficient can now determined by adjusting its value until the location where $S_o=S_f$ corresponds to the location at which $G^2=1$. An example of the numerical spreadsheet is given in Appendix B.

6.4 Interface Profile

The interface profile assumed for the analysis (Equation 6.1) was derived from frictionless theory (Lawrence 1990b). An analysis is done using the experimental data to attempt to reevaluate the profile and the interfacial friction coefficient.

Starting with Equation 4.20, a slope of the interface at the throat is estimated from the experimental data. At the throat, the topographical slope, $S_o=0$ and height of the interface, $y_2'= ½$. Using the value of f_I determined from the original model as a first estimate, the slope of the interface can be reevaluated at the next increment of x and subsequently along the length of the channel. The initial slope at the throat and f_I are adjusted until $S_o=S_f$ at the point where $G^2=1$.

7. DISCUSSION ON THE INTERFACIAL FRICTION COEFFICIENT

Although previous work suggests that the magnitude of the interfacial friction coefficient is small relative to the wall friction coefficient, this is not necessarily the case as shown by the numerical work of which the results are discussed in §8.3. In fact, from the numerical and experimental work the interfacial friction is of the same order of magnitude as the wall friction from the Blasius Equation. Bertelsen and Warren (1977) also state that the interfacial shear stress has proved to be of greater importance than expected in the movement of the lower layer.

Dermisses and Partheniades (1984) summarized prior prominent investigations of Keulegan (1949), Ippen and Harleman (1951), Abraham and Eysink (1971), and Lofquist (1960) and found that a wide discrepancy among graphical and analytical equations for f_I exist. After applying some of these equations to the same problem, Dermisses and Partheniades found that f_I may in fact differ by orders of magnitude. There are also differing opinions as to the appropriate dimensionless parameters to use in correlating f_I. For example, Keulegan introduced as criterion, the Keulegan Number which is a function of the Reynolds and Densimetric Froude numbers. Other authors have also taken this approach including Macagno and Rouse (1962) as well as Shi-Igai (1965). However, Abraham and Eysink, Ippen and Harleman, and Lofquist all came to the conclusion that f_I is a

function of the Reynolds Number only, with Lofquist's and Ippen and Harleman's results being extremely similar with $f_I = 139/Re$ (Lofquist) and $f_I = 140/Re$ (Ippen and Harleman). Grubert (1990) follows the work of Keulegan and Lofquist. Using data from the South Pass of the Mississippi River (arrested salt wedge situation) he concludes that $f/8 = 0.012\ R^{-1/4}$. Since f here is the Darcy coefficient then the interfacial friction coefficient $f_I = 0.012\ R^{-1/4}$

Dermisses and Partheniades conducted experiments in a rectangular duct and came to the conclusion that f_I can best be correlated with the Reynolds number and a regular nondensimetric Froude number together as RF^2 as well as with the relative density difference, $\Delta\rho/\rho$. They present a family of curves based on these parameters which are in close agreement with both their laboratory data and field data from the Mississippi estuary. Explicitly expressed is their conclusion that neither the densimetric Froude number nor the Reynolds numbers can be used as single correlation parameters.

Eidnes (1986) presents a method for determining the interfacial friction coefficient based on a Richardson number for pressure driven shear flow for a top stationary and a bottom flowing layer of fluid and suggests that $f_I = 2.63*10^{-3}/Ri$ where Ri is a gradient Richardson number, $Ri = g'y/\Delta u^2$. Note that this Richardson number is indeed the inverse of the stability Froude number defined earlier (3.11) and that f_I is

proportional to F_Δ^2 which is proportional to the height of the instabilities which can be regarded as roughness. Eidnes states that the corresponding values for a bottom current are stated to be 1.6 times higher and stipulates that this equation is valid only for Ri<10.

Bertelsen and Warren (1977) suggest a value of $f_I = 0.001$ or approximately half of the bed stress coefficient, f_w. This is a result of calibrating data taken from the Danish Belts, applied to their computer simulation of two-layer flows. Di Silvio (1975) used a constant value for the Darcy coefficient of 0.05 which is equivalent to a f_I value of 0.0062. Calibration of this coefficient came from data of the Adige River in N.E. Italy.

Macagno (1962) presents a more rigorous derivation for rectangular pipe flow of what he terms the resistance coefficient based on density and velocity profiles and the geometry of the system. He derives an equation for this situation based on the hydraulic radius, Rh, the width, b, and the displacement thickness, δ, and the wetted perimeter, P. An attempt to correlate the resistance coefficient with the Froude and Reynolds numbers was made; however, although a definite correlation was apparent, no distinctive quantitative conclusion was drawn.

Numerous Japanese authors have examined the friction coefficient in great detail. Still many seem to agree with or

approve of earlier works done by Kaneko in the early 1950's. Kaneko correlates the interfacial friction coefficient with the Froude and Reynolds numbers as many others have subsequently done and introduces the parameter Ψ, where $\Psi = ReFr^2$ and the interfacial friction coefficient, $f_I=0.2\Psi^{-\frac{1}{4}}$.

Georgiev (1990) states that f_I should depend on the type of flow (bottom density current, arrested salt wedge or exchange flow), the Reynolds number and the stability characteristics quantified by a densimetric Froude number he defines by Fr'. Georgiev defines the Reynolds number, $Re = u_2Rh/\nu$ and the densimetric Froude number, $Fr' = u_2^2/(g'Rh)$ where Rh is the hydraulic radius with wetted perimeter that includes not only the walls and surface but also the interface. He also attempted to plot a relation of the interfacial friction coefficient with Re and shows curves of constant Fr' that can be examined as curves of constant roughness. Recall that f_I is proportional to F_Δ^2 which is proportional to the instability height which can be regarded as a roughness. Values of the interfacial friction coefficient from his data ranged from 0.0006 to 0.008. Using the relation plotted by Georgiev would suggest a value of f_I in the present study of approximately 0.004.

Although many authors have used field data to arrive at a value for the interfacial friction coefficient and some also present formulas based on such data, it is still inconclusive as to how to calculate such a coefficient. The present objective

is not to try to identify which of the methods are suitable for determining the interfacial coefficient, but rather to test whether the results of the present study give values that are comparable to other methods previously published and perhaps present a numerical approach to calculating the interfacial friction coefficient. Therefore a comprehensive review was done using several of the above mentioned methods which are summarized in Table I.

Table I: Summary of Interfacial Friction Coefficients

Author	Formulation	Conditions
Ippen	$f_I = 140/Re$	Laminar underflows
Grubert	$f_I = 0.012\ Re^{-1/4}$	Stratified estuaries and fjords
Eidnes	$f_I = 4.21(10^{-3})/Ri$	Bottom flowing layer Ri < 10
Macagno	$f_I = 4g'/u^2\ (Rh-b\delta/4P)$	Pipe flow Experimental
Kaneko	$f_I = 0.2\ \psi^{-1/4}$	Salt wedge Experimental

A graph showing these various coefficients is plotted as a function of Reynold's Number (Figure 12). Shown are values calculated from the 5 equations given in Table I using data from several of the experiments conducted, constant values suggested by Di Silvio and Georgiev, along with the experimental values

determined from the numerical model. It is interesting to note in Table I that Grubert's equation is based on field data and the others equations on experimental data. The results of using his equation give the largest values for the interfacial friction coefficient. Perhaps this is due to the use of field data which would imply larger Reynolds numbers in the field as opposed to the laboratory and this would be reflected in his correlation.

8. RESULTS AND DISCUSSION

8.1 Hydraulic Solutions

The stability Froude number is vital to the analysis of exchange flows and with the inclusion of frictional effects it is found that $F_\Delta^2<1$. Since this is the case, Long's stability criterion is satisfied for long internal waves and confidence can be placed in the internal hydraulic theory.

Using experimental data from Experiment #18 reveals the relation of the three pertinent Froude numbers: the composite Froude number, the internal Froude number and the stability Froude number (see Figure 13). The Froude numbers are calculated using Equations 3.7, 3.10, and 3.11 respectively and plotted against the nondimensional length of the contracted channel, x'. Notice that F_Δ^2 is constant throughout the channel length and the control point is located where $G^2=1$ which coincides with $F_I^2=1$. These values are calculated assuming a velocity reduction or flow ratio of experimental values to frictionless theory (Equation 6.2), of k = 0.74.

A comparison plot of Equation 6.1, the calculated theoretical height of the interface, and the height of the interface measured from various experiments is given in Figure 14. Although good agreement can be seen near the channel ends, there is some deviation from the theoretical values just on either side of the throat. Given the difficulty in determining the position of the interface due to movement and the presence

of instabilities, these values match the frictionless profile remarkably well.

Reevaluation of the interface profile using Equation 4.20 to include frictional effects reveals little difference in the shape of the profile and does not appear to improve the match of the experimental data either. A plot of both the frictionless and reevaluated frictional profiles is shown in Figure 15a along with the variation of So, Sf, and $1-G^2$ in Figure 15b. With frictional effects included in reevaluation of the profile, the location of the control points were pushed farther along the channel close to the channel ends. Entrance and exit effects may explain some of the discrepancy between the model and the experimental data. Refinement of the experimental profile through more exact data collection may be needed before a precise experimental profile can be assumed.

The long term variation of the interface height at the throat taken from photographs and video recordings is shown in Figure 16. Although theoretically the interface height at the throat, y_2', is assumed to be ½, there appears to be an oscillation about the mid-depth. It is not clear as to the cause of these deviations; however, it is proposed that they may be caused by the apparatus itself by a period of "rebound" or circulation which is a function of the size of the end reservoirs.

8.2 Flow visualization

The use of slide projectors to attain a two-dimensional image of the two-layer flow experiment was extremely successful. Photographs of the experiment resulted in good visualization of both the Kelvin-Helmholtz and Holmboe instabilities at the interface. Several series of photographs are shown in Figures 17 through 21. Growth and development of Kelvin-Helmholtz billows can be seen in Figures 17, 18, and 19. In Figure 17 (Experiment #19), the throat is located on the left edge of the ruler visible near the center of the photographs. The series of photographs in Figure 18 taken from Experiment #24 show a transition from a fairly smooth interface to the development of much turbulence at the interface. The photographs are taken of the left channel with the throat located at the edge of the ruler on the right side on the photographs. Again the growth of Kelvin-Helmholtz billows is shown in Figure 19 (Experiment #25) showing a series of photographs taken of the channel to the left of the throat.

A series of both Kelvin-Helmholtz and Holmboe instabilities can be seen in Figure 20 photographed centered at the throat of the channel from Experiment #21. The development of Holmboe instabilities are shown in Figure 21 beginning with a single cusp and the last photograph showing 4 cusps. Distinct wavelengths of the Holmboe mode are taken from these photographs.

A final interface thickness was obtained from the photographs and video recordings of the experiments. Figure 22, originally presented by Lawrence (1990b), is shown with several data points from the present study added. As best as can be determined, $\delta_{max}'=0.15\pm0.05$, but varies for each experiment. Variation of the dimensionless maximum interface thickness δ'_{max} with the stability Froude number are shown in Figure 22 with lines indicating values of the bulk Richardson number, $J = g'\delta/\Delta u^2$.

A photograph of the interface thickness is shown in Figure 23 taken from Experiment #23 with the throat at the right side of the photograph. The interface thickness can also clearly be seen in the long exposure photograph (Figure 7).

Wavelengths of both the Holmboe and Kelvin-Helmholtz modes of instability are measured from photographs of the experiments. A photograph showing wavelengths of Kelvin-Helmholtz mode is given in Figure 24. These wavelengths and calculated values of the stability parameters are given in Table II.

Table II. Calculated Stability Parameters

Exp #	h (cm)	J	λ (cm)	α
18	3.20	0.20	18.0	1.12
19	3.70	0.23	17.0	1.37
20	3.50*	0.22	18.2	1.21
21	3.50*	0.22	16.4	1.34
22	3.53	0.22	21.1	1.05
23	3.53	0.22	29.3	0.76
24	3.80*	0.23	29.4	0.81
25	3.80*	0.23	33.1	0.72

* Estimated from Video Recordings or Photographs

$J=g'h/(\Delta u)^2$
$\alpha=2\pi/\lambda$
λ=average wavelength for experiment

Koop and Browand (1979) determined a value of J=0.32 from their experiments. Note that the value of J in the present study varies from 0.20 to 0.23 with Reynold's numbers being larger than (6 to 8 times) those of Koop and Browand's experiments. However, Koop and Browand (1979) also state that the maximum Richardson number decreases to as little as 0.15 with increasing initial Richardson numbers.

Figure 25 is a stability diagram plotted by Lawrence, Browand & Redekopp (1990) where α here is the instability wave number, α = kh, k = $2\pi/\lambda$, and λ is the wavelength. Additional explanation of the stability diagram is given by Lawrence et al (1990). Also shown on the diagram are the wavelengths measured

from the experiments. Note that all of the data points lie within the region predicting the instabilities. The possibility of pairing of the billows might explain the higher values of λ and therefore lower values of α which is consistent with the points plotted in Figure 25.

Although photographs were used to initially obtain velocity profiles, using a video recording of the experiment proved to be the more complete and accurate method of obtaining velocity profiles. An example long exposure photograph showing the streaks left by the beads used for velocities was shown in Figure 7.

8.3 Interfacial Friction Coefficient

From the experimental and numerical work conducted it is shown that for the situation of exchange flow, the interfacial friction coefficient is of the same order of magnitude and several times larger than the wall friction. On average, the interfacial friction, f_I=0.0088 for β=1.0 and as high as 0.0096 for β=0. The variation of α, where $\alpha=f_I/f_w$, with the velocity coefficient, k, determined numerically from the data of Experiment #22 is shown in Figure 26 allowing for three surface conditions of β: 0, 0.5 and 1. The significance of the surface friction is small as can be seen by the relative difference of the three curves. Values of both the interfacial friction and wall friction coefficients along with additional experimental data for all experiments are given in Table III.

Table III: Experimental Data and Friction Coefficients

Exp #	bo cm	y cm	g' cm/s2	vel. Eq.6.3 cm/s	u exp cm/s	Rh cm	Re (Rh)	Re (x)	f	fw f/8	fI
1	10.2	16.8	2.48	3.23	2.39	3.17	2316	18246	0.020	0.0025	0.0047
2	10.0	26.1	1.85	3.47	2.57	3.61	2834	19602	0.019	0.0024	0.0082
3	5.5	27.8	1.50	3.23	2.39	2.30	1676	18246	0.020	0.0025	0.0093
4	5.5	28.6	1.51	3.29	2.43	2.31	1715	18585	0.019	0.0024	0.0094
5	10.6	28.2	1.26	2.98	2.21	3.85	2594	16834	0.020	0.0026	0.0088
6	10.6	26.0	0.99	2.70	2.00	3.77	2297	15252	0.022	0.0027	0.0093
7	10.5	29.5	0.99	2.70	2.00	3.87	2362	15252	0.022	0.0027	0.0093
8	10.5	29.5	0.86	2.52	1.86	3.87	2205	14235	0.022	0.0028	0.0096
9	10.3	29.5	0.94	2.64	1.95	3.82	2277	14913	0.022	0.0027	0.0094
10	10.1	29.3	1.10	2.85	2.11	3.76	2418	16099	0.021	0.0026	0.0094
11	10.1	29.6	1.53	3.37	2.49	3.77	2867	19037	0.019	0.0024	0.0096
13	10.4	29.5	0.94	2.64	1.95	3.84	2293	14913	0.022	0.0027	0.0095
14	10.3	29.7	0.94	2.64	1.95	3.82	2281	14913	0.022	0.0027	0.0095
15	10.3	29.7	0.94	2.64	1.95	3.82	2281	14913	0.022	0.0027	0.0095
16	10.5	29.6	1.05	2.78	2.06	3.88	2434	15704	0.021	0.0026	0.0097
18	10.4	29.6	1.02	2.74	2.03	3.85	2382	15478	0.021	0.0027	0.0097
	Viscosity =		1.31	(10-2) cm/s2			(10 C)				
19	10.7	29.6	1.46	3.29	2.43	3.93	2676	17025	0.020	0.0025	0.0101
20	10.6	29.5	1.29	3.09	2.29	3.90	2494	15990	0.021	0.0026	0.0100
21	10.6	29.5	0.98	2.69	1.99	3.90	2171	13920	0.023	0.0028	0.0098
	Viscosity =		1.43	(10-2) cm/s2			(7 C)				
22	10.4	28.8	1.77	3.57	2.64	3.82	4037	18474	0.020	0.0024	0.0099
23	10.4	29.4	1.77	3.57	2.64	3.84	4059	18474	0.020	0.0024	0.0102
24	10.5	29.6	1.72	3.57	2.64	3.88	4095	18474	0.020	0.0024	0.0103
25	10.5	29.6	1.72	3.57	2.64	3.88	4095	18474	0.020	0.0024	0.0103
	Viscosity =		1.00	(10-2) cm/s2			(21 C)				

Experimental velocities are 74% of theoretical

The full wetted perimeter has been included

f = 2.656/sqrt(Rex)	Wall friction factor (Eq. 6.3)
fw = f/8	Standardized wall friction factor
beta = 0	
Re(Rh) = 4Rh u/viscosity	Reynolds number based on hydraulic radius
Re(x) = uL/viscosity	Reynolds number based on channel length

Note that the value of f_I for experiment #1 is lower than that of the other experiments. This is due to the shallow depth of this experiment which restricts growth of the billows and hence lowers the effective roughness and results in a lower f_I.

A theoretical relation between k and α was derived using conditions at the throat. Although this is may not be appropriate for the whole channel, it provides a good first estimate of the value of the interfacial friction factor. Figure 27 show the theoretical curves calculated. Note again the small difference in the three curves for the entire range of β indicating that the surface friction has little impact on the determination of the interfacial friction coefficient. Details of the theoretical derivation are given in Appendix C. A comparison plot of the theoretical and experimental relation between k and α is shown in Figure 28 for the case, β=0.

Although some previous authors have elected to ignore or assume very small values for the interfacial friction in the theory of layered flows, it is shown by the numerical and experimental work that it is pertinent to the theory and should be included in any analysis.

8.4 Control Point Location

With estimates of the interfacial, wall, and surface friction coefficients, the hydraulic equations derived can be used to help locate the control points of a two-layer exchange flow. After determining the location of the controls for each

experiment from the numerical model using a frictionless interface profile as discussed in §6, it was found that the controls were located between x'=±0.40 and x'=±0.45. However, after reevaluation of the interface to include friction the controls were located within the vicinity of the ends of the contraction (x'=±0.55). Depending on the velocity reduction coefficient, k, that was used, the location of the controls varies within this region. After examining the velocity profiles both across the width of the channel and throughout the depth of the channel, a value of k=0.74±0.05 was found to be appropriate. For k=0.74, the controls were located at x'=±0.51 (f_i=0.0104, Exp. #18) and for k=0.70, x'=±0.68 (f_I=0.0130).

With the consideration of frictional effects, the control points of an exchange flow do not occur at the narrowest section as suggested by inviscid theory but lie on either side of the throat and perhaps at the ends of the contraction. Still the controls must satisfy the singularity condition G^2=1 and are separated by a region of subcritical flow. The relation of the control points and the composite Froude number is diagrammed in Figure 29 calculated from Experiment #5. Illustrated are the two control points on either side of the throat separated by a region of subcritical flow (G^2<1). At the two controls, the composite Froude number takes on a value of unity. Beyond the control points, the flow becomes supercritical (Figure 29a). A theoretical interface profile along the channel is shown in Figure 29b. The Froude number plane showing the location of the

control points (b_c) and the throat (b_o) relative to the Froude numbers for each layer is given in Figure 29c.

9. CONCLUSION

The interfacial friction coefficient is of great importance to the analysis of layered flows especially in the locating of the hydraulic controls. The addition of frictional considerations moves the theoretical location of the control points away from the throat of the contraction. For the experiments conducted the control points were calculated to be located in the vicinity of the ends of the contraction. A value of 0.74 ± 0.05 for the velocity reduction coefficient was determined from the data analyzed and resulted in an average interfacial friction factor of 0.0096 (β=0) and 0.0088 (β=1.0) using a frictionless interface profile. These values increase with the use of the frictional profile by approximately 7%.

The ability to obtain good flow visualization both through photographs and video recordings has definitely proven worthy in order to obtain more accurate data for testing the hydraulic theory. Visualization of the interface provides data for better understanding as well as additional observation of the phenomenon of both the Kelvin-Helmholtz and Holmboe instabilities. The theoretical profile (Equation 6.1) is shown to be adequate in estimating the height of the interface along the channel.

Measurements of the maximum interface thickness are found to agree with the variation of the thickness and the stability Froude number presented by Lawrence (1989). As well, the measurements made of the instability wavelengths found in the

experiments lie within the predicted region of interfacial instability occurrence given by Lawrence et al (1990).

10. RECOMMENDATIONS

The use of a larger facility with a more flexible apparatus may help to obtain additional data particularly for higher Reynold's numbers to further examine the hydraulic theory. As well, additional field data is needed to test the theory in large scale situations.

A more extensive review of existing data on the interfacial friction coefficient is still needed. To attain and assemble together all existing data to try and achieve some sort of correlation in the results may be necessary. An emphasis may include field data and categorization of different types of flow and the resulting interfacial friction coefficients.

It is difficult to obtain an accurate profile of the interface along the entire channel due to its length. A more precise method of obtaining this profile is needed to refine the analysis if increased accuracy is required. It is suggested that vertical profiles of the density be taken using conductivity probes at multiple location along the channel. Variation of f_w along the channel, as a constant value was assumed may also help to increase the accuracy of results.

The analysis may be approached by assuming the controls of the experiment occur at the ends of the contraction and calculate in toward the throat. This requires the slope of the interface at the control points and hence the use of L'Hopital's rule to differentiate Equation 4.20 which is beyond the scope of the present study.

Bibliography

Armi, L. (1986). "The hydraulics of two flowing layers with different densities", J. Fluid Mech., **Vol. 163**, pp. 27-58.

Armi, L. and Farmer, D.M. (1986). "Maximal two-layer exchange through a contraction with barotropic net flow", J. Fluid Mech., **Vol. 164**, pp. 27-51.

Armi, L. and Farmer, D.M. (1988). "The flow of Mediterranean water through the Strait of Gibraltar", Prog. Oceanogr. **Vol. 21.**

Assaf, G. and Hecht, A. (1974). "Sea straits: a dynamical model", Deep-Sea Research, **Vol. 21,** pp. 947-958.

Baines, P.G. and Guest, F. (1988). "The nature of upstream blocking in uniformly stratified flow over long obstacles", J. Fluid Mech., **Vol. 188**, pp. 23-45.

Benton, G.S. (1954). "The occurrence of critical flow and hydraulic jumps in a multi-layered fluid system", J. Met., **Vol. 11**, pp. 139-150.

Bertelsen, J.A. and Warren, I.R. (1977). "Two-layer modelling of the Danish belts: collection and processing of data and calibration of the models", IAHR, pp. 379-386.

Christodoulou, G.C. (1986). "Interfacial mixing in stratified flows", J. Hyd. Res., **Vol. 24**, No. 2., pp. 77-89.

Denton, R.A. (1986). "Locating and identifying hydraulic controls for layered flow through an obstruction", J. Hyd. Res., **Vol. 25**, No. 3, pp. 281-299.

Denton. R.A. (1990). "Classification of unidirectinal three-layer flow over a hump", J. Hyd. Res., **Vol. 28,** No. 2, pp. 215-233.

Dermisses, V. and Partheniades, E. (1984). "Interfacial resistance in stratified flows", ASCE Waterway, Port and Ocean Engineering, **Vol. 110**, pp. 231-250.

Di Silvio, G. (1975). "Calibration of a mathematical model for the stratified salt intrusion in tidal river mouths", IAHR, Sao Paolo, pp. 284-292.

Eidnes, G. (1986). "Interfacial mixing in stationary, pressure-driven flow", ASCE, pp. 322-334.

Farmer, D.M. and Armi, L. (1986). "Maximal two-layer exchange over a sill and through the combination of a sill and contraction with barotropic flow", J. Fluid Mech., **Vol. 164**, pp. 53-76.

Farmer, D.M. and Armi, L. (1988). "The flow of Atlantic water through the Strait of Gibraltar", Prog. Oceanogr. **Vol. 21.**

Georgiev, B.V. (1990). "On the interface phenomena in two-layer stratified flow", Proc. of the International Conf. on Physical modelling of Transport and Dispersion, IAHR/ASCE, E.E. Adams & G.E. Hecker Eds., MIT August 7-10, 1990., pp. 4B.7-4B.12.

Goldstein, S. (1931). "On the stability of superposed streams of fluid of different densities", Proc. Roy. Soc. A., **Vol. 132,** pp. 524-548.

Grubert, J.P. (1990). "Interfacial mixing in estuaries and fjords", J. of Hydraulic Engineering, **Vol. 116**, No. 2, pp. 176-195.

Hamblin, P.F. and Lawrence, G.A. (1990). "Exchange flows between Hamilton Harbour and Lake Ontario", Proc. of the 1990 Conference of the CSCE, **Vol. V,** pp. 140-148.

Hansen, N.E.O. and Moeller, J.S. (1990). "Zero blocking solution for the Great Belt Link", The Physical Oceanography of Sea Straits (L.J. Pratt, ed.), NATO/ASI Series, Klewer, Dordrecht.

Henderson, F.M. (1966). "Open Channel Flow", Macmillan Publishing Co.

Hino, M., Hung, N.S., and Nakamura, K. (1980). "Entrainment and friction at the interface of salt wedge", Second International Symposium on Stratified Flows, Norway, pp. 763-782.

Koop, C.G. and Browand, F.K. (1979). "Instability and turbulence in a stratified fluid with shear", J. of Fluid Mech., **Vol. 93**, pp. 135-159.

Lai, K.K. and Wood, I.R. (1975). "A two layer flow through a contraction", J. Hyd. Res., IAHR, **Vol. 13**, pp. 19-34.

Lawrence, G.A. (1985). "Mixing in steady two-layer flow over topography", Ph.D. Thesis, University of California, Berkeley.

Lawrence, G.A. (1990a). "On the hydraulics of Boussinesq and non-Boussinesq two-layer flows", J. Fluid Mech., **Vol. 215**, pp. 457-480.

Lawrence, G.A. (1990b). "Can mixing in exchange flows be predicted using internal hydraulics?", The Physical Oceanography of Sea Straits (L.J. Pratt, ed.), NATO/ASI Series, Klewer, Dordrecht.

Lawrence, G.A., Browand, B.K. & Redekopp, L.G. (1990). "The stability of a sheared density interface", Physics of Fluids A: Fluid Dynamics, In Press.

Lawrence, G.A. and Cheung, E.A. (1989). "An experimental study of exchange through a convergent-divergent contraction", EOS, **Vol. 70**, No. 43, pp 1167.

Lawrence, G.A. and Cheung, E.A. (1990). "Internal hydraulics, interfacial stability and mixing in exchange flow through a contraction", Proc. of the International Conf. on Physical modelling of Transport and Dispersion, IAHR/ASCE, E.E. Adams & G.E. Hecker Eds., MIT August 7-10, 1990., pp. 8A.13.

Long, R.R. (1956). "Long waves in a two-fluid system", J. Met. **13**, pp. 70.

Macagno, E.O., and Rouse, H. (1962). "Interfacial mixing in stratified flow" Transactions of the ASCE, **Vol. 127**, Part I, pp. 102-128.

Schijf, J.B. and Schönfeld, J.C. (1953). "Theoretical considerations on the motion of salt and fresh water", Proc. of the Minn. Int. Hydraulics Conv., Joint meeting IAHR and Hyd. Div ASCE., **Sept. 1953**, pp. 321-333.

Schlichting, H. (1979). "Boundary-Layer Theory", McGraw-Hill.

Sherman, F.S., Imberger, J., Corcos, G.M. (1978). "Turbulence and mixing in stably stratified waters", Annual Rev. Fluid Mech., **Vol. 10**, pp. 267-288.

Shi-Igai, H. and Sawamoto, M. (1969). "Experimental and theoretical modelling of saline wedges", IAHR, **Vol. 3**, C4-1 - C4-7.

Smyth, W.D., Klassen, G.P., and Peltier, W.R. (1988). "Finite amplitude Holmboe waves", Geophys. Astrophys. Fluid Dynamics, **Vol. 43**, pp. 181-222.

Smyth, W.D. and Peltier, W.R. (1989). "The transition between Kelvin-Helmholtz and Holmboe instability: an investigation of the overreflection hypothesis", J. of the Atmospheric Sciences, **Vol. 46**, No. 24, pp. 3698-3720.

Taylor, G.I. (1931). "Effect of variation in density on the stability of wuperposed streams of fluid", Proc. Roy. Soc. A., **Vol. 132**, pp. 499-523.

Thomson, R.E. (1981). "Oceanography of the British Columbia coast", Can. Spec. Publ. Fish. Aquat. Sci., **56.**

Thorpe, S.A. (1987). "Transitional phenomena and the development of turbulence in stratified fluids: A review", J. of Geophysical Research, **Vol. 92**, No. C5, pp. 5231-5248.

Turner, J.S. (1973). "Bouyancy effects in fluids", Cambridge University Press.

Wilkinson, D.L. and Wood, I.R. (1983). "The formation of an intermediate layer by horizontal convection in a two-layered shear flow", J. Fluid Mech., **Vol. 136**, pp. 167-187.

Wood, I.R. (1970). "A lock exchange flow", J. Fluid Mech., **Vol. 42**, pp. 671-687.

Appendix A

Derivation of the Equation of the Slope of the Interface

From Equation 4.13:

$$\boldsymbol{C}\frac{\partial v}{\partial x} = \boldsymbol{D}\frac{\partial f}{\partial x} + S \qquad (4.13)$$

rearranging

$$\frac{\partial v}{\partial x} = \boldsymbol{C}^{-1}\boldsymbol{D}\frac{\partial f}{\partial x} + \boldsymbol{C}^{-1}\boldsymbol{S}$$

again where v(x), D, f(x), and S are given by

$$\boldsymbol{v} = \begin{bmatrix} u_1 \\ u_2 \\ y_1 \\ y_2 \end{bmatrix} \quad \boldsymbol{D} = \begin{bmatrix} -g & 0 \\ -g & 0 \\ 0 & Q_1 \\ 0 & Q_2 \end{bmatrix} \quad \boldsymbol{f} = \begin{bmatrix} h_s \\ b^{-1} \end{bmatrix} \quad \boldsymbol{S} = \begin{bmatrix} -f_w\frac{u_1^2}{b} - f_I\Delta u^2\frac{1}{y_1} - f_s u_1^2\frac{1}{y_1} \\ f_w u_2^2\left(\frac{2}{b}+\frac{1}{y_2}\right) + f_I\Delta u^2\frac{1}{y_2} \end{bmatrix}$$

Since we are primarily interested in the height of the interface, only the last component of matrix **v** will be shown here. The first term on the right hand side is evaluated

$$\boldsymbol{C}^{-1}\boldsymbol{D}\frac{\partial f}{\partial x} = \left[\frac{F_1^2-1}{1-G^2}\right]\frac{dh_s}{dx} + \left[\frac{G^2-F_1^2\left(1+\frac{ry_1}{y_2}\right)}{1-G^2}\right]\frac{y_2}{b}\frac{db}{dx}$$

and the second term:

$$\boldsymbol{C}^{-1}\boldsymbol{S} = \frac{2f_w}{b}\left[\frac{F_1^2y_1+F_2^2y_2}{1-G^2}\right] + f_w\left[F_2^2\right] + f_s\left[F_1^2\right] + f_I F_\Delta^2\left[\frac{y^2}{y_1y_2}\right]$$

Note that $\mathbf{C}^{-1}\mathbf{S}$ is defined as ΔS_f given in Equation 4.18. Adding together the preceeding two equations gives

$$\frac{dy_2}{dx} = \left[\frac{G^2-F_1^2(1+ry_1/y_2)}{1-G^2}\right]\frac{y_2}{b}\frac{db}{dx} - \left[\frac{1-F_1^2}{1-G^2}\right]\frac{dh_s}{dx} + \left[\frac{\Delta S_f}{1-G^2}\right]$$

and moving y_2 to the left hand side results in Equation 4.17.

APPENDIX B

EXPERIMENTAL CALCULATIONS FOR EXPERIMENT # 18

Experimental Data

u =	2.03 cm/sec	Uth	=	2.74 cm/sec		r	=	0.9989
bo =	10.4 cm	k	=	0.74		epsi	=	0.0010
y =	29.6 cm							
g' =	1.02 cm/s2	fw	=	0.0027				
qo =	30.0 cm2/sec	fi	=	0.0097				
		alpha	=	3.6				
Q =	312 cm3/sec	x inc	=	0.01				

x'	b'	y1'	y2'	y1	y2	b	u1	u2	F1sq	F2sq	Gsq	Fdsq	So	fw terms	fi terms	Sf	So-Sf
0.00	1	0.50	0.50	14.80	14.80	10.4	2.03	2.03	0.27	0.27	0.545	0.54	0.0000	0.0007	0.0211	0.0219	0.0219
0.01	1.000	0.50	0.50	14.95	14.65	10.40	2.01	2.05	0.26	0.28	0.545	0.54	0.0000	0.0007	0.0211	0.0219	0.0219
0.02	1.000	0.51	0.49	15.10	14.50	10.40	1.99	2.07	0.26	0.29	0.546	0.54	0.0001	0.0008	0.0211	0.0220	0.0220
0.03	1.000	0.51	0.49	15.24	14.36	10.40	1.97	2.09	0.25	0.30	0.547	0.54	0.0001	0.0008	0.0211	0.0220	0.0219
0.04	1.001	0.52	0.48	15.39	14.21	10.41	1.95	2.11	0.24	0.31	0.548	0.54	0.0003	0.0009	0.0212	0.0221	0.0219
0.05	1.002	0.52	0.48	15.54	14.06	10.42	1.93	2.13	0.23	0.32	0.550	0.54	0.0004	0.0009	0.0212	0.0222	0.0218
0.06	1.003	0.53	0.47	15.69	13.91	10.43	1.91	2.15	0.23	0.33	0.553	0.54	0.0006	0.0010	0.0212	0.0223	0.0217
0.07	1.004	0.53	0.47	15.83	13.77	10.45	1.89	2.17	0.22	0.34	0.555	0.54	0.0008	0.0011	0.0212	0.0223	0.0216
0.08	1.006	0.54	0.46	15.98	13.62	10.46	1.87	2.19	0.21	0.35	0.559	0.54	0.0010	0.0011	0.0213	0.0224	0.0214
0.09	1.008	0.54	0.46	16.13	13.47	10.48	1.85	2.21	0.21	0.36	0.562	0.54	0.0013	0.0012	0.0213	0.0225	0.0213
0.10	1.010	0.55	0.45	16.28	13.32	10.50	1.83	2.23	0.20	0.37	0.567	0.54	0.0016	0.0012	0.0213	0.0226	0.0211
0.11	1.012	0.55	0.45	16.42	13.18	10.52	1.81	2.25	0.19	0.38	0.571	0.54	0.0019	0.0013	0.0214	0.0227	0.0208
0.12	1.014	0.56	0.44	16.57	13.03	10.55	1.79	2.27	0.19	0.39	0.576	0.54	0.0023	0.0013	0.0214	0.0228	0.0206
0.13	1.017	0.56	0.44	16.72	12.88	10.57	1.77	2.29	0.18	0.40	0.582	0.54	0.0027	0.0014	0.0215	0.0229	0.0203
0.14	1.019	0.57	0.43	16.86	12.74	10.60	1.75	2.31	0.18	0.41	0.588	0.54	0.0031	0.0015	0.0215	0.0231	0.0200

0.15	1.022	0.57	0.43	17.01	12.59	10.63	1.73	2.33	0.17	0.42	0.594	0.54	0.0036	0.0015	0.0216	0.0232	0.0196
0.16	1.025	0.58	0.42	17.15	12.45	10.66	1.71	2.35	0.17	0.43	0.601	0.54	0.0041	0.0016	0.0217	0.0233	0.0193
0.17	1.029	0.58	0.42	17.30	12.30	10.70	1.69	2.37	0.16	0.45	0.609	0.54	0.0046	0.0016	0.0217	0.0234	0.0189
0.18	1.032	0.59	0.41	17.44	12.16	10.74	1.67	2.39	0.16	0.46	0.616	0.54	0.0052	0.0017	0.0218	0.0236	0.0184
0.19	1.036	0.59	0.41	17.59	12.01	10.78	1.65	2.41	0.15	0.47	0.625	0.54	0.0058	0.0018	0.0219	0.0237	0.0180
0.20	1.040	0.60	0.40	17.73	11.87	10.82	1.63	2.43	0.15	0.49	0.634	0.54	0.0064	0.0018	0.0220	0.0239	0.0175
0.21	1.045	0.60	0.40	17.87	11.73	10.86	1.61	2.45	0.14	0.50	0.643	0.54	0.0070	0.0019	0.0221	0.0240	0.0170
0.22	1.049	0.61	0.39	18.02	11.58	10.91	1.59	2.47	0.14	0.52	0.653	0.54	0.0077	0.0020	0.0222	0.0242	0.0165
0.23	1.054	0.61	0.39	18.16	11.44	10.96	1.57	2.49	0.13	0.53	0.663	0.54	0.0084	0.0020	0.0223	0.0243	0.0160
0.24	1.059	0.62	0.38	18.30	11.30	11.01	1.55	2.51	0.13	0.55	0.674	0.54	0.0092	0.0021	0.0224	0.0245	0.0154
0.25	1.064	0.62	0.38	18.44	11.16	11.07	1.53	2.53	0.12	0.56	0.685	0.54	0.0099	0.0021	0.0225	0.0247	0.0148
0.26	1.069	0.63	0.37	18.58	11.02	11.12	1.51	2.55	0.12	0.58	0.697	0.54	0.0107	0.0022	0.0226	0.0249	0.0142
0.27	1.075	0.63	0.37	18.72	10.88	11.18	1.49	2.57	0.12	0.59	0.709	0.54	0.0115	0.0023	0.0227	0.0251	0.0136
0.28	1.081	0.64	0.36	18.86	10.74	11.24	1.47	2.58	0.11	0.61	0.722	0.54	0.0124	0.0023	0.0229	0.0252	0.0129
0.29	1.087	0.64	0.36	19.00	10.60	11.31	1.45	2.60	0.11	0.63	0.736	0.54	0.0133	0.0024	0.0230	0.0254	0.0122
0.30	1.094	0.65	0.35	19.14	10.46	11.37	1.43	2.62	0.11	0.64	0.750	0.54	0.0142	0.0025	0.0231	0.0257	0.0115
0.31	1.100	0.65	0.35	19.28	10.32	11.44	1.41	2.64	0.10	0.66	0.764	0.54	0.0151	0.0025	0.0233	0.0259	0.0108
0.32	1.107	0.66	0.34	19.42	10.18	11.52	1.40	2.66	0.10	0.68	0.780	0.54	0.0161	0.0026	0.0234	0.0261	0.0100
0.33	1.115	0.66	0.34	19.55	10.05	11.59	1.38	2.68	0.09	0.70	0.795	0.54	0.0171	0.0027	0.0236	0.0263	0.0093
0.34	1.122	0.67	0.33	19.69	9.91	11.67	1.36	2.70	0.09	0.72	0.812	0.54	0.0181	0.0028	0.0237	0.0265	0.0085
0.35	1.130	0.67	0.33	19.83	9.77	11.75	1.34	2.72	0.09	0.74	0.829	0.54	0.0192	0.0028	0.0239	0.0268	0.0077
0.36	1.138	0.67	0.33	19.96	9.64	11.83	1.32	2.73	0.09	0.76	0.846	0.54	0.0202	0.0029	0.0241	0.0270	0.0068
0.37	1.146	0.68	0.32	20.09	9.51	11.92	1.30	2.75	0.08	0.78	0.864	0.54	0.0213	0.0030	0.0242	0.0273	0.0060
0.38	1.155	0.68	0.32	20.23	9.37	12.01	1.28	2.77	0.08	0.80	0.883	0.54	0.0225	0.0031	0.0244	0.0275	0.0051
0.39	1.164	0.69	0.31	20.36	9.24	12.10	1.27	2.79	0.08	0.83	0.903	0.54	0.0236	0.0031	0.0246	0.0278	0.0042
0.40	1.173	0.69	0.31	20.49	9.11	12.20	1.25	2.81	0.07	0.85	0.923	0.54	0.0248	0.0032	0.0248	0.0281	0.0033
0.41	1.183	0.70	0.30	20.62	8.98	12.30	1.23	2.83	0.07	0.87	0.943	0.54	0.0260	0.0033	0.0250	0.0283	0.0024
0.42	1.192	0.70	0.30	20.75	8.85	12.40	1.21	2.84	0.07	0.90	0.965	0.54	0.0272	0.0034	0.0252	0.0286	0.0014
0.43	1.203	0.71	0.29	20.88	8.72	12.51	1.19	2.86	0.07	0.92	0.987	0.54	0.0285	0.0034	0.0254	0.0289	0.0005
0.44	1.213	0.71	0.29	21.01	8.59	12.62	1.18	2.88	0.06	0.95	1.010	0.54	0.0298	0.0035	0.0257	0.0292	-0.0005
0.45	1.224	0.71	0.29	21.14	8.46	12.73	1.16	2.90	0.06	0.97	1.034	0.54	0.0311	0.0036	0.0259	0.0295	-0.0015
0.46	1.235	0.72	0.28	21.26	8.34	12.85	1.14	2.91	0.06	1.00	1.058	0.54	0.0324	0.0037	0.0261	0.0299	-0.0025
0.47	1.247	0.72	0.28	21.39	8.21	12.97	1.12	2.93	0.06	1.03	1.083	0.54	0.0337	0.0038	0.0264	0.0302	-0.0035

APPENDIX B continued: Refinement of Main Spreadsheet

Program to compute the value of the velocity coefficient, k, from
the Shear equations where G2=1 @ So=Sf
Initial conditions for Experiment # 25

gprime	=	1.72	cm/s2	bo	=	10.5	cm
Utheor	=	3.57	cm/sec	H	=	29.6	cm
viscos	=	0.01	cm/s2	L	=	110	cm
Reynold	=	4701					
fw	=	0.0024		alpha=fi/fw		xprime=x/2L	
alpha	=	4.29		beta=fs/fw		Sf=Sfw+Sfb+Sfi	
beta	=	0		y={1+sqrt[(1-k^2)/(1+3k^2)]}/2			
fi	=	0.0103					
fs	=	0.0023					

k	y (y2)	b'	x/2L	F1sq	F2sq	Gsq	Sfw	Sfb	Sfi	Sf	So	So-Sf	k	x'
0.730	0.71	1.22	0.45	0.938	0.062	1.0	0.0012	0.0001	0.03	0.0286	0.0298	-0.0011884	0.730	0.445
0.732	0.71	1.22	0.44	0.937	0.062	1.0	0.0012	0.0002	0.03	0.0287	0.0296	-0.0009478	0.732	0.443
0.734	0.71	1.21	0.44	0.936	0.063	1.0	0.0013	0.0002	0.03	0.0288	0.0295	-0.0007056	0.734	0.440
0.736	0.71	1.21	0.44	0.935	0.064	1.0	0.0013	0.0002	0.03	0.0289	0.0293	-0.0004617	0.736	0.438
0.738	0.71	1.21	0.44	0.934	0.065	1.0	0.0013	0.0002	0.03	0.0290	0.0292	-0.0002162	0.738	0.436
0.740	0.71	1.21	0.43	0.933	0.066	1.0	0.0013	0.0002	0.03	0.0291	0.0291	0.00003079	0.740	0.433
0.742	0.71	1.20	0.43	0.933	0.067	1.0	0.0013	0.0002	0.03	0.0292	0.0289	0.00027948	0.742	0.431
0.744	0.70	1.20	0.43	0.932	0.068	1.0	0.0013	0.0002	0.03	0.0293	0.0288	0.00052976	0.744	0.429
0.746	0.70	1.20	0.43	0.931	0.069	1.0	0.0013	0.0002	0.03	0.0294	0.0286	0.00078164	0.746	0.426

Appendix C

Derivation of k and α relation

Starting with Equation 4.20

$$\frac{dy_2}{dx} = \frac{S_o - \Delta S_f}{1 - G^2} \qquad (4.20)$$

at the throat, $S_o = 0$, therefore,

$$\frac{dy_2}{dx} = \frac{\Delta S_f}{1 - G^2}$$

From the interface profile we can appoximate dy_2/dx by its slope at the throat, y/4L, determined from the frictionless interface profile (Equation 6.1) such that

$$\frac{y}{4L} = \frac{\Delta S_f}{1 - G^2}$$

At the throat, we know that

$$G^2 = k^2$$

$$F_1^2 = F_2^2 = \frac{k^2}{2}$$

$$y_1 = y_2 = \frac{y}{2}$$

$$\frac{y^2}{y_1 y_2} = \frac{y^2}{y^2/4} = 4$$

such that

$$(1-k^2)\frac{y}{4L} = \frac{2f_w}{b}\left[\frac{k^2}{2}\frac{y}{2}+\frac{k^2}{2}\frac{y}{2}\right] + f_w\frac{k^2}{2} = 4f_I k^2 = f_s\frac{k^2}{2}$$

$$(1-k^2)\frac{y}{4L} = \frac{f_w}{b}k^2 y + (f_w+f_s)\frac{k^2}{2} + 4f_I k^2$$

Rearranging, we finally get a relation for f_i and k.

$$f_I = \frac{(1-k^2)y}{16k^2 L} - f_w\left(\frac{1}{8}+\frac{y}{4b}\right) - \frac{f_s}{8}$$

Note the relationship plotted in Figure 27 is k and α, where $\alpha = f_i/f_w$.

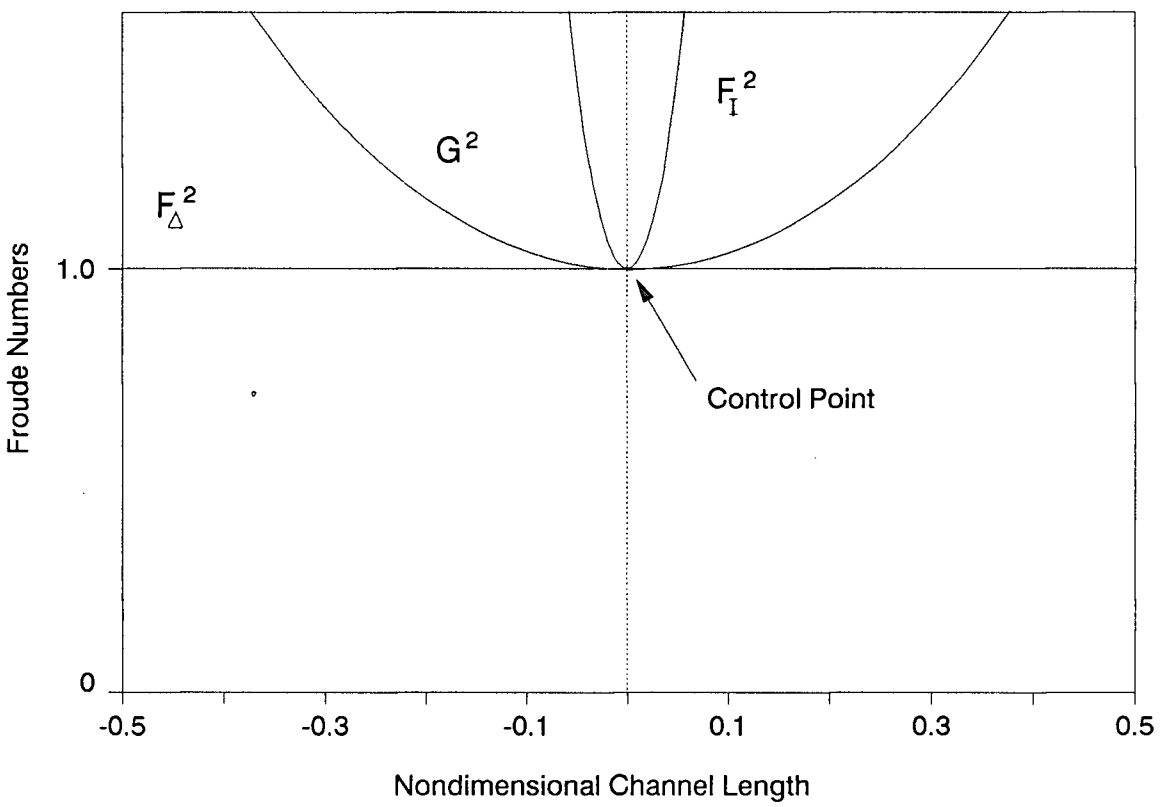

Figure 1. Variation of the internal, composite and stability Froude numbers throughout a contracted channel for inviscid flows

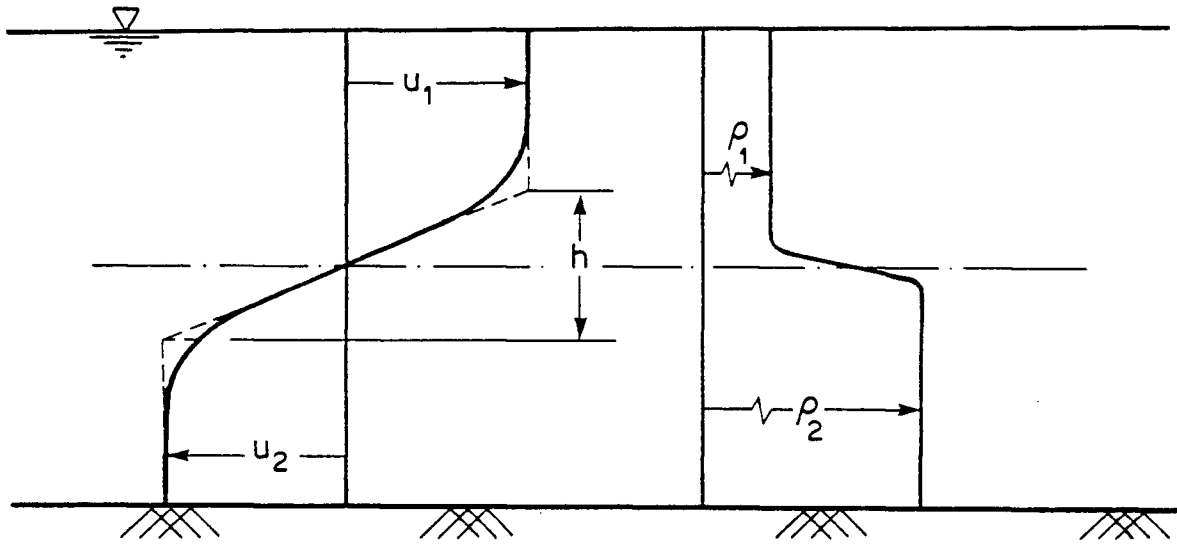

Figure 2. Definition sketch of assumed linear approximations of both the velocity and density profiles

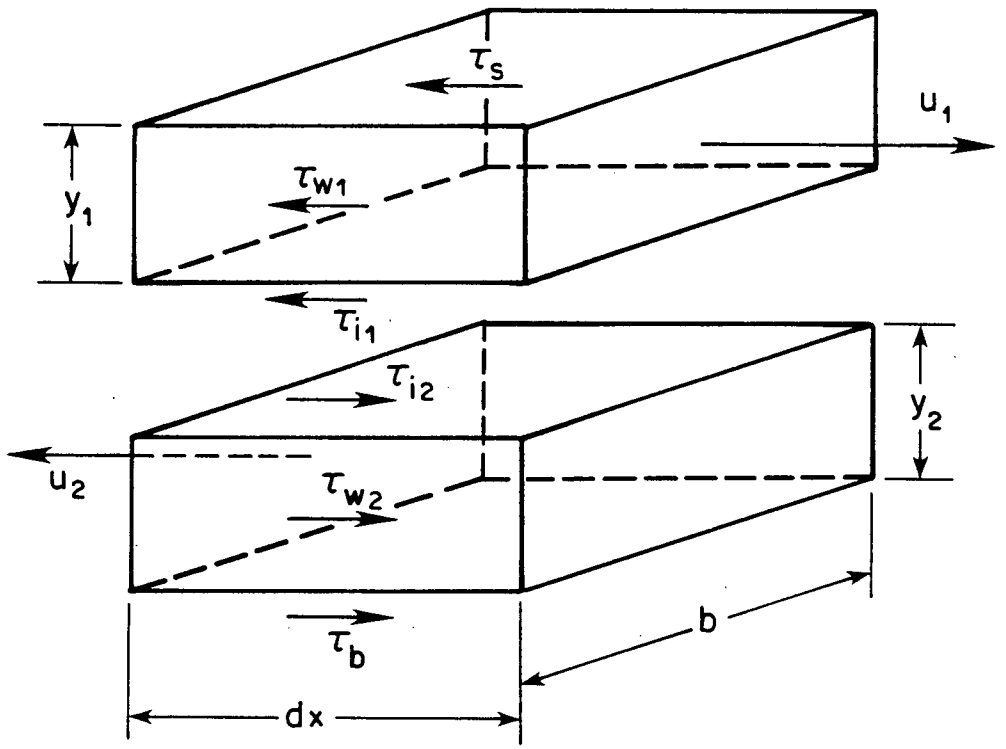

Figure 3. Definition sketch of the shear stresses acting on a volume of fluid for both the upper and lower layers

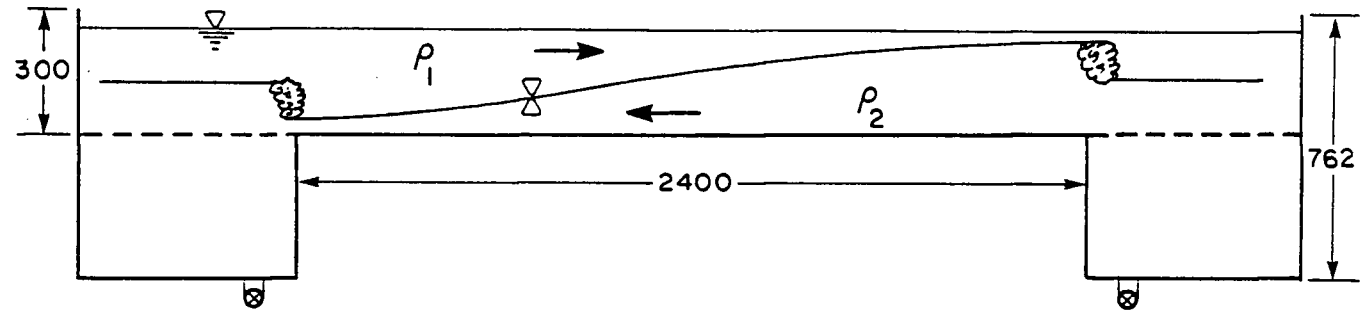

ELEVATION

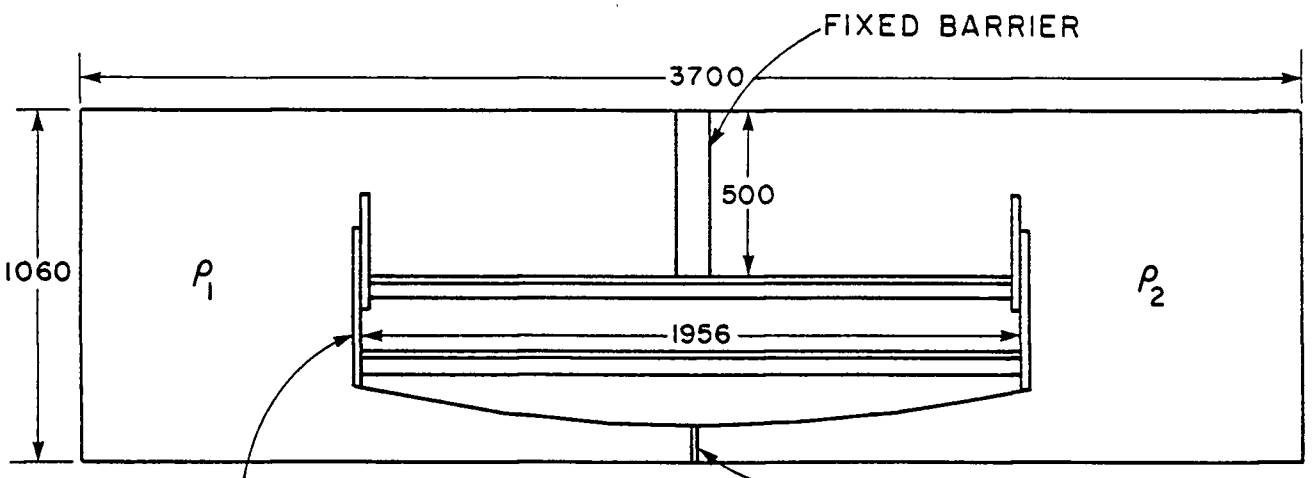

PLAN

Figure 4. Experimental set-up (all dimensions in millimeters)

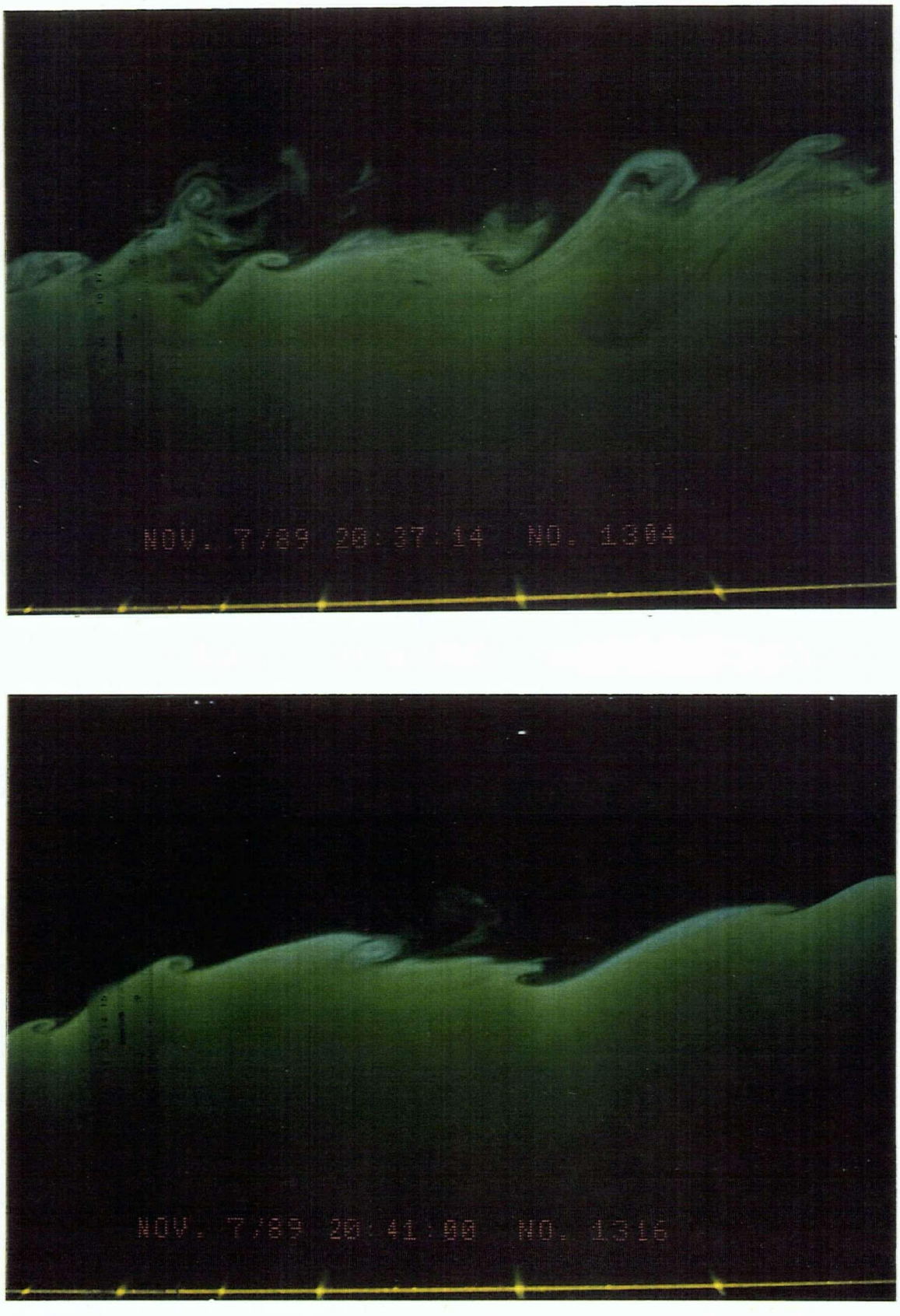

Figure 5. Photographs of the experiment in progress

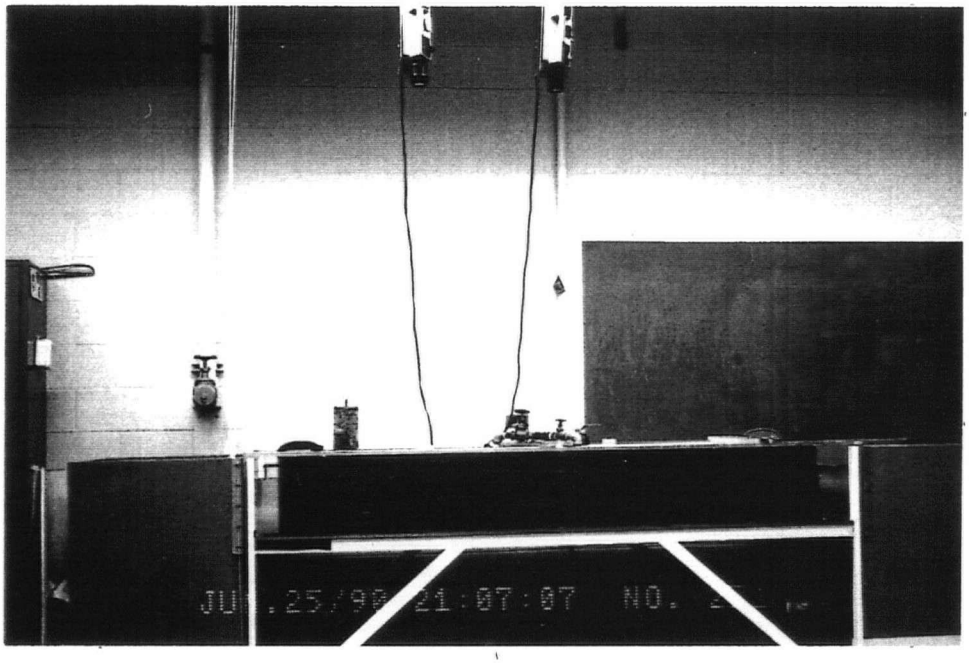

Figure 6. Photograph of the experimental apparatus

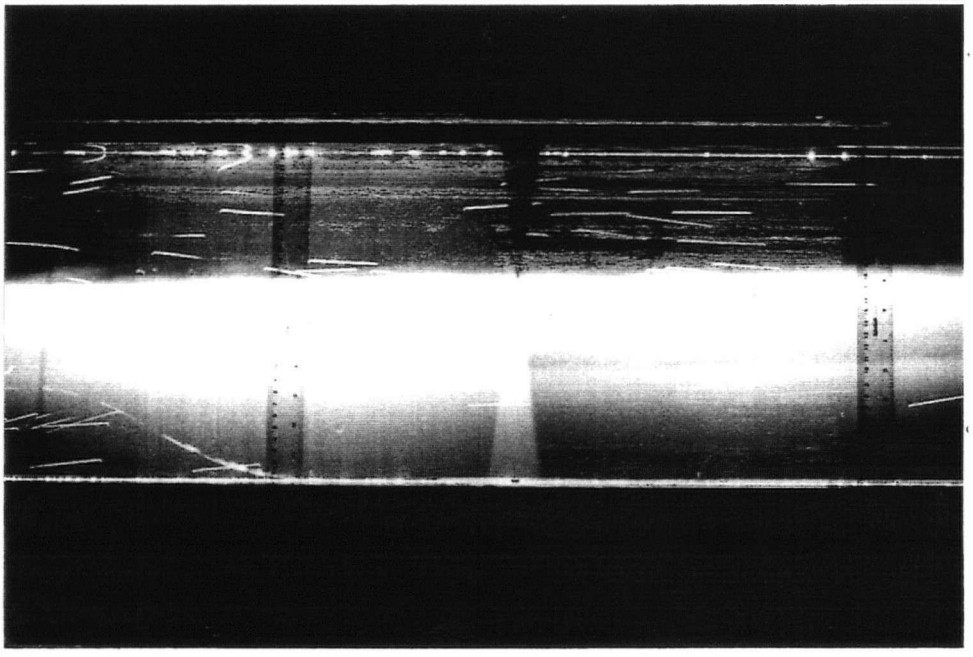

Figure 7. Long exposure photograph showing movement of velocity beads

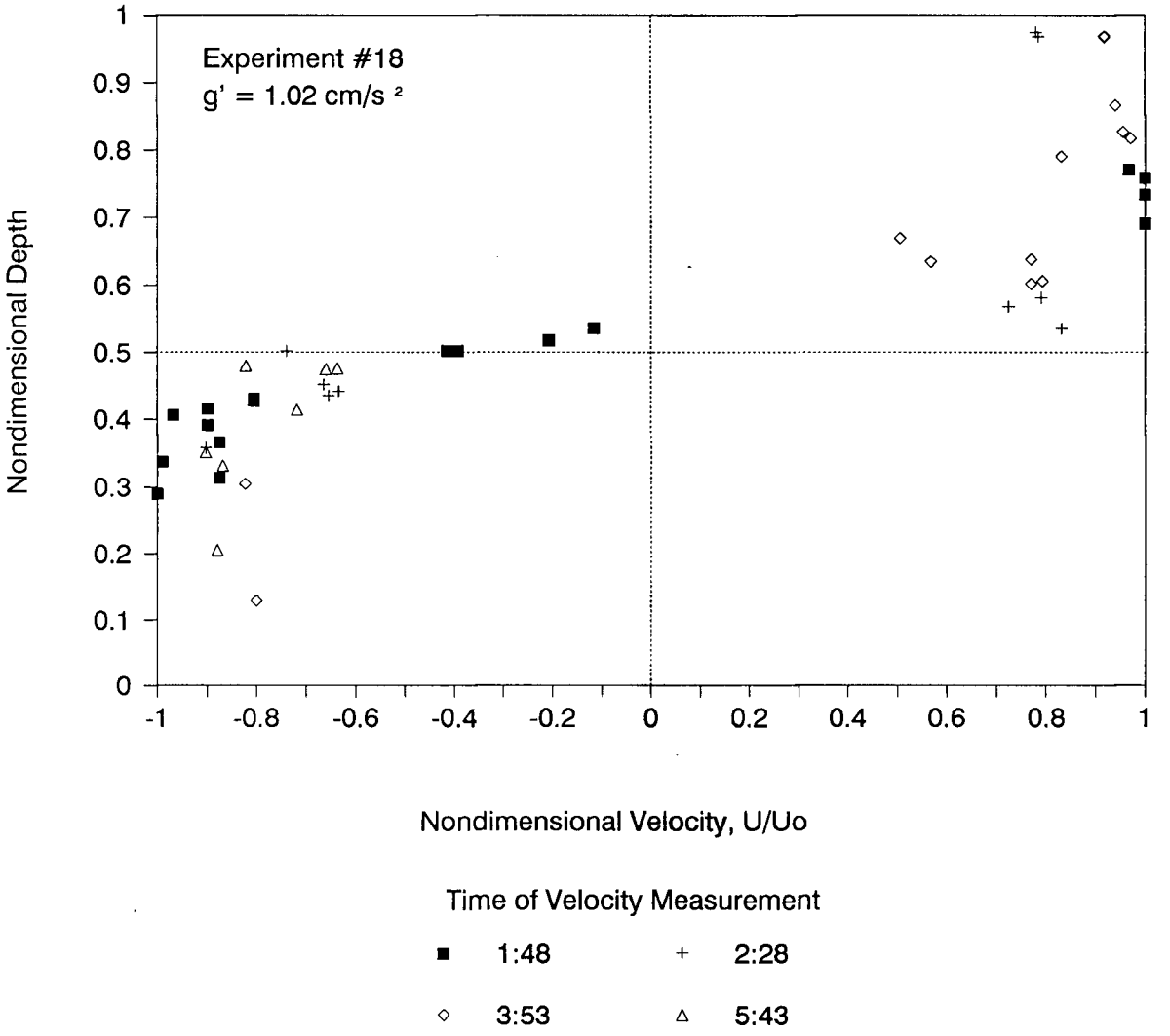

Figure 8. Velocity Profile at the throat for Experiment #18

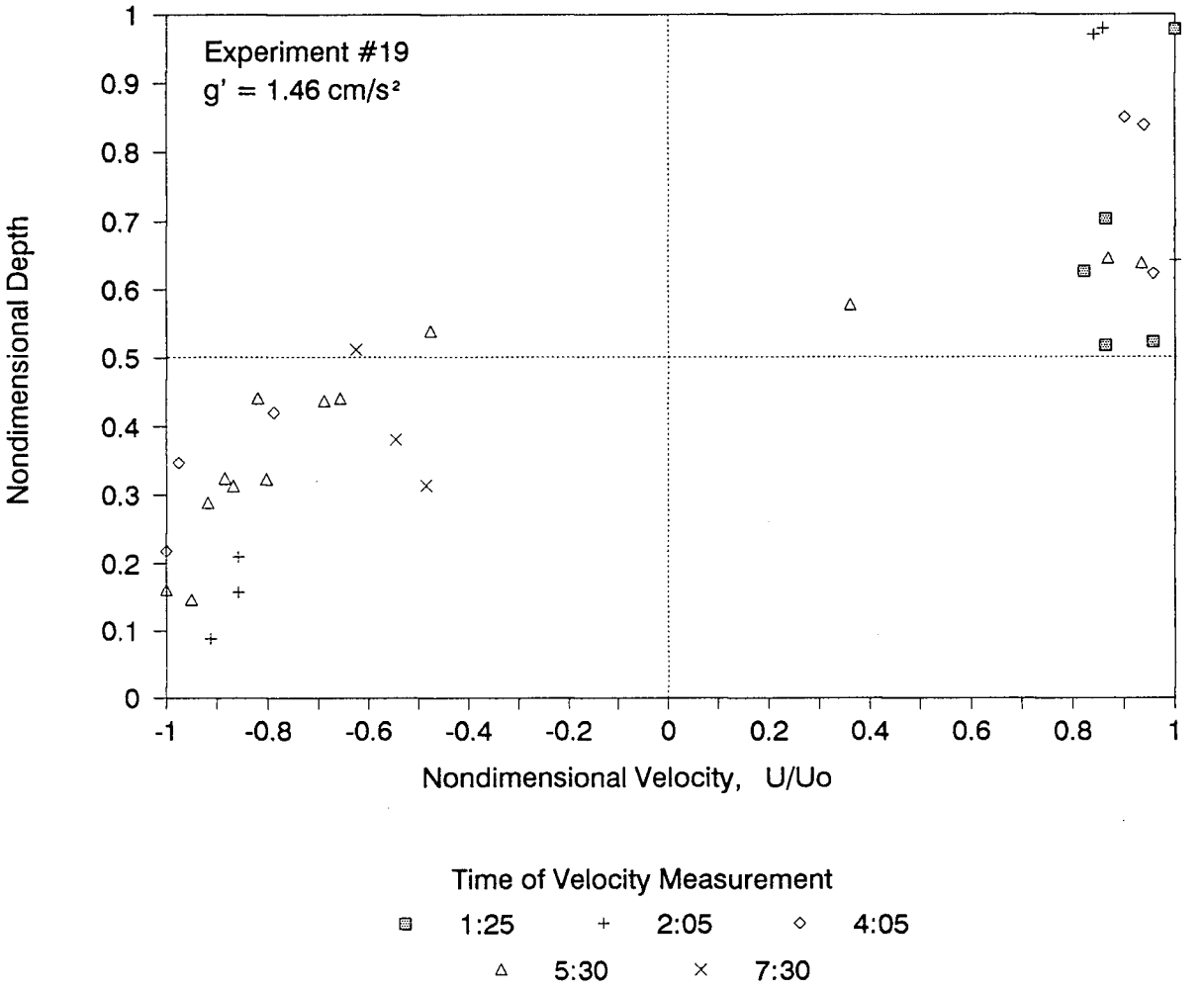

Figure 9. Velocity profile at the throat for Experiment #19

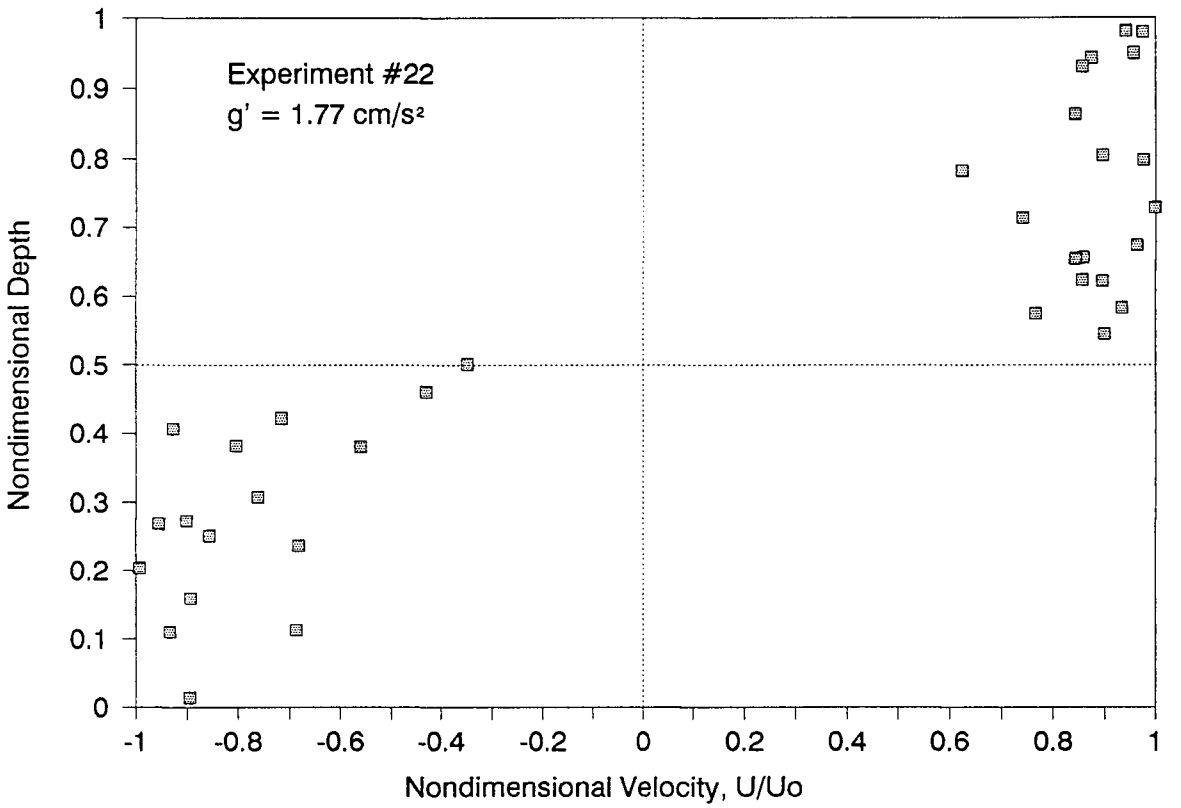

Figure 10. Velocity profile at the throat for Experiment #22

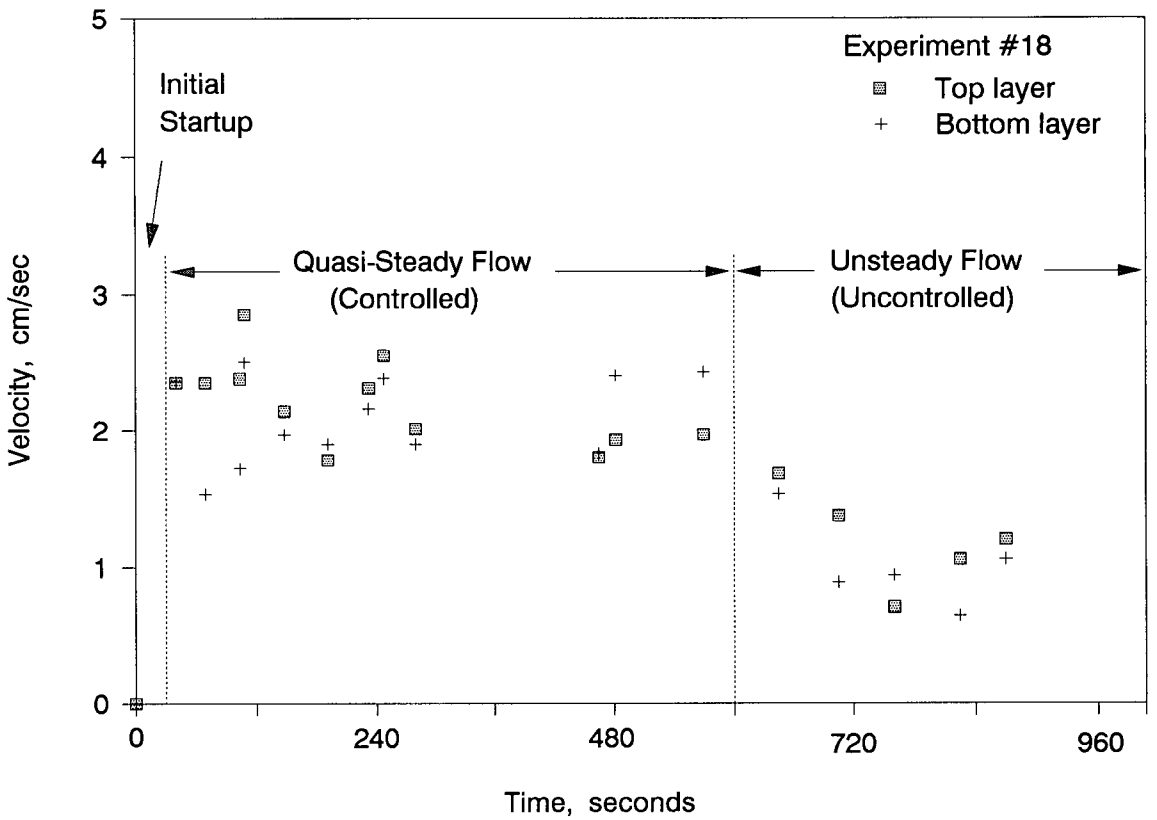

Figure 11. Long term variation of the average velocity at the throat for Experiment #18

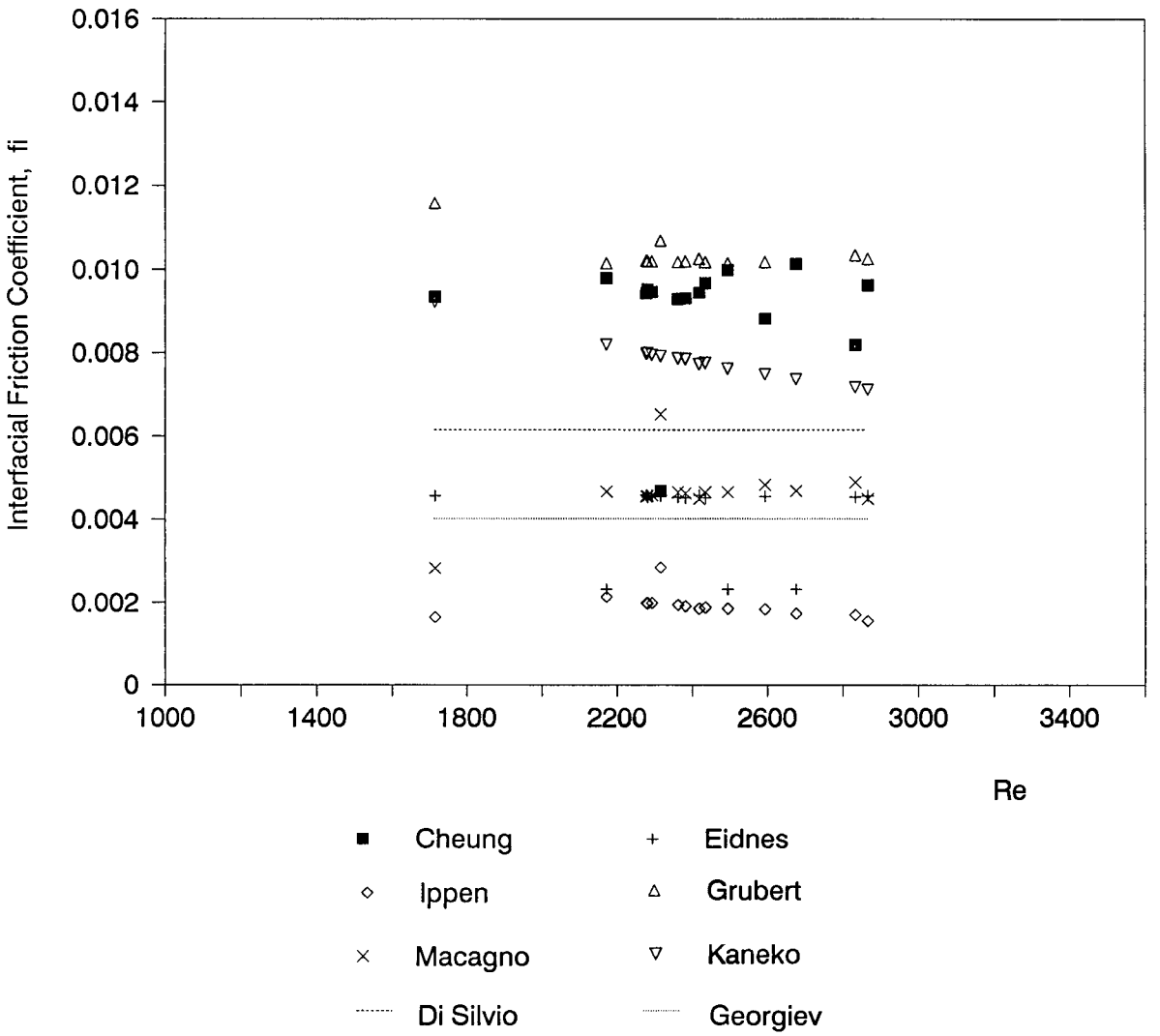

Figure 12. Comparison of various interfacial friction coefficients plotted as a function of Reynolds number

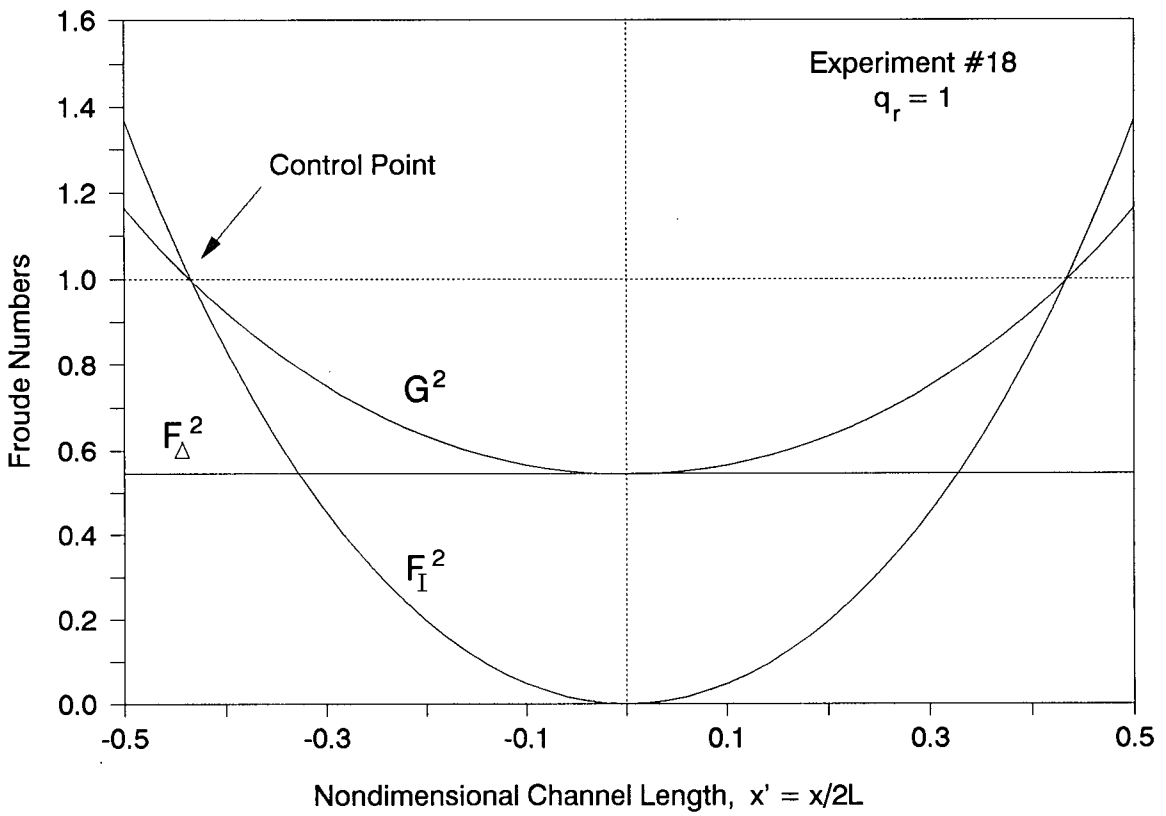

Figure 13. Variation of the internal, composite and stability Froude numbers throughout the contracted channel

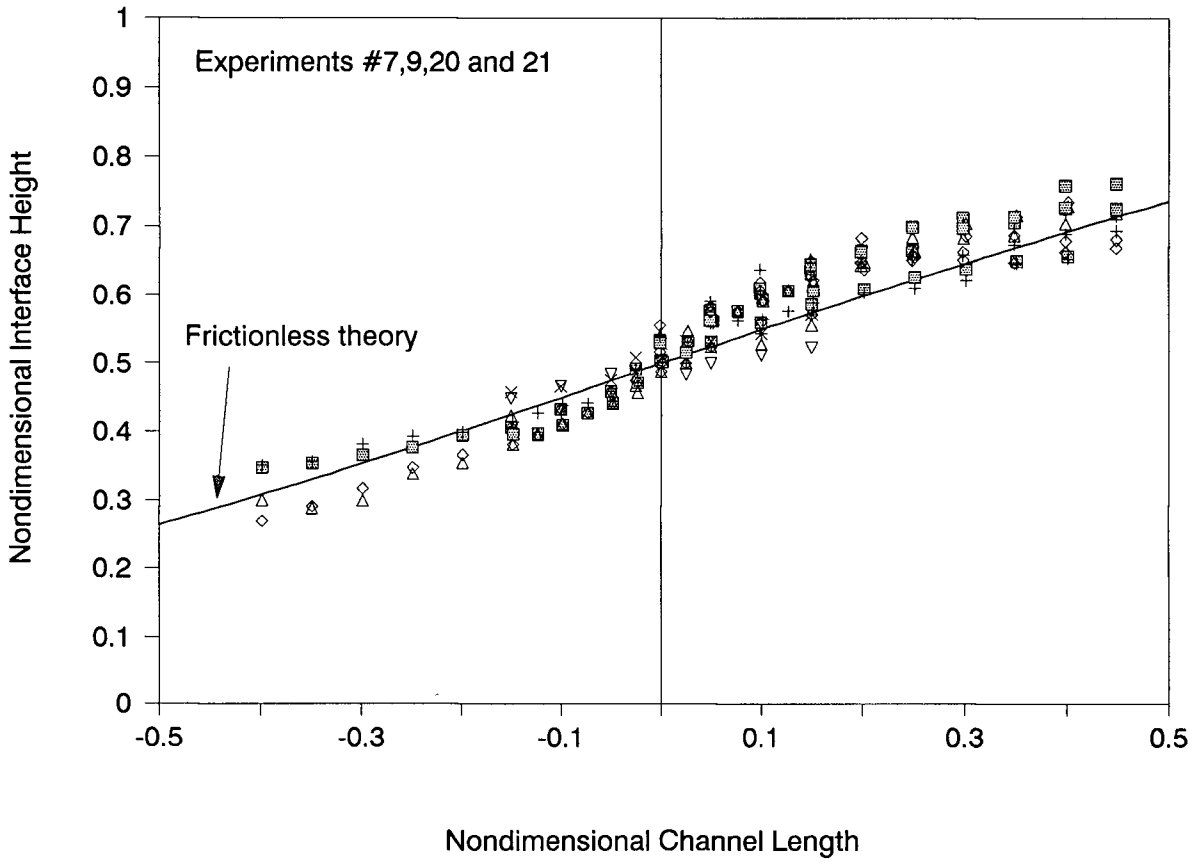

Figure 14. Comparison plot of the experimental and theoretical interface height along the channel

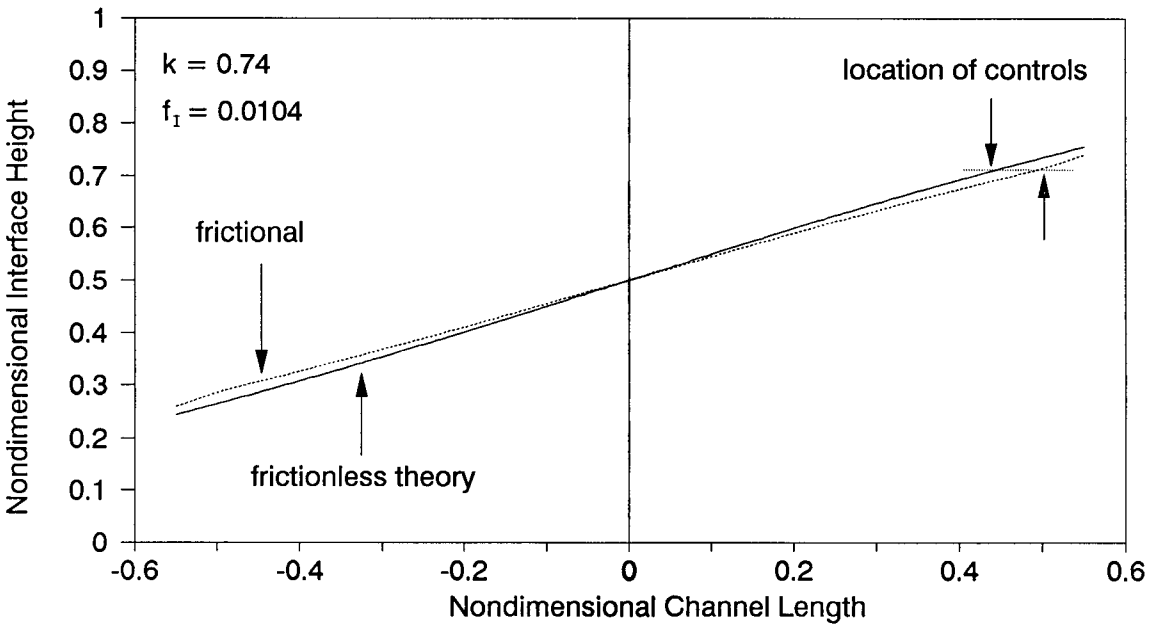

Figure 15a. Comparison of frictionless and friction interface profiles

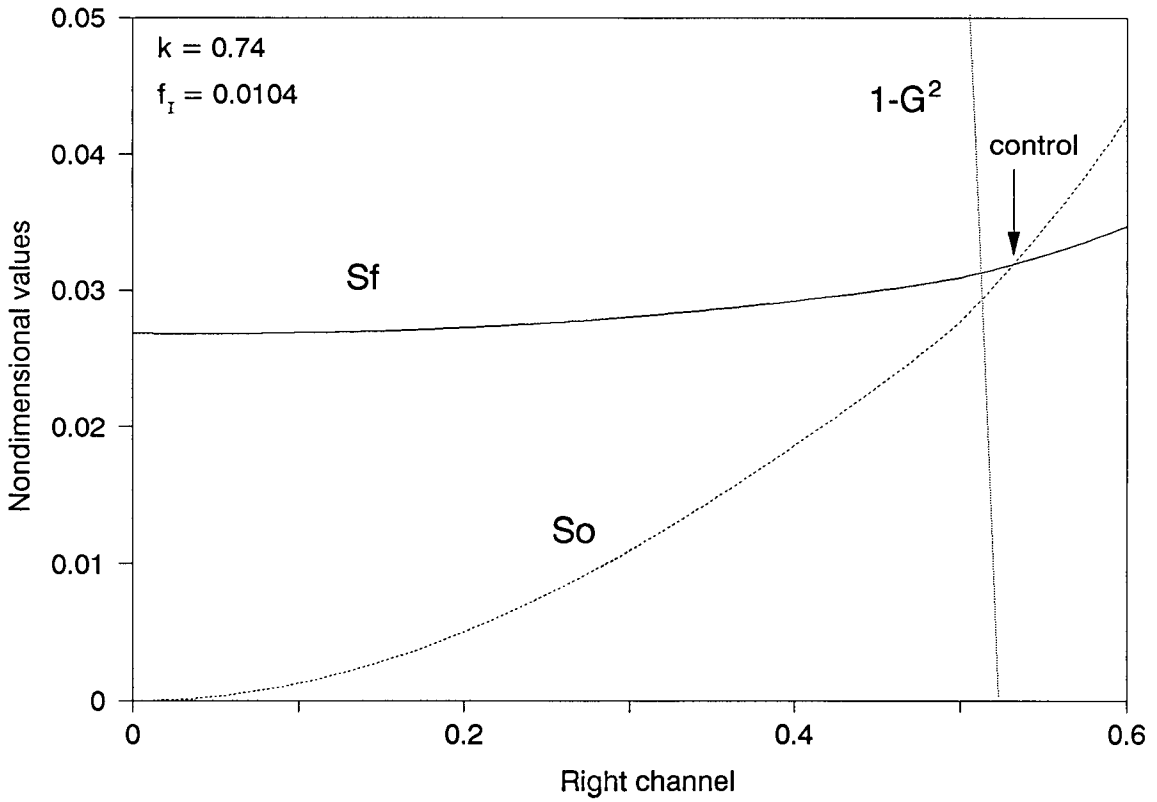

Figure 15b. Variation of Sf, So and 1-G ^{2} approaching the control

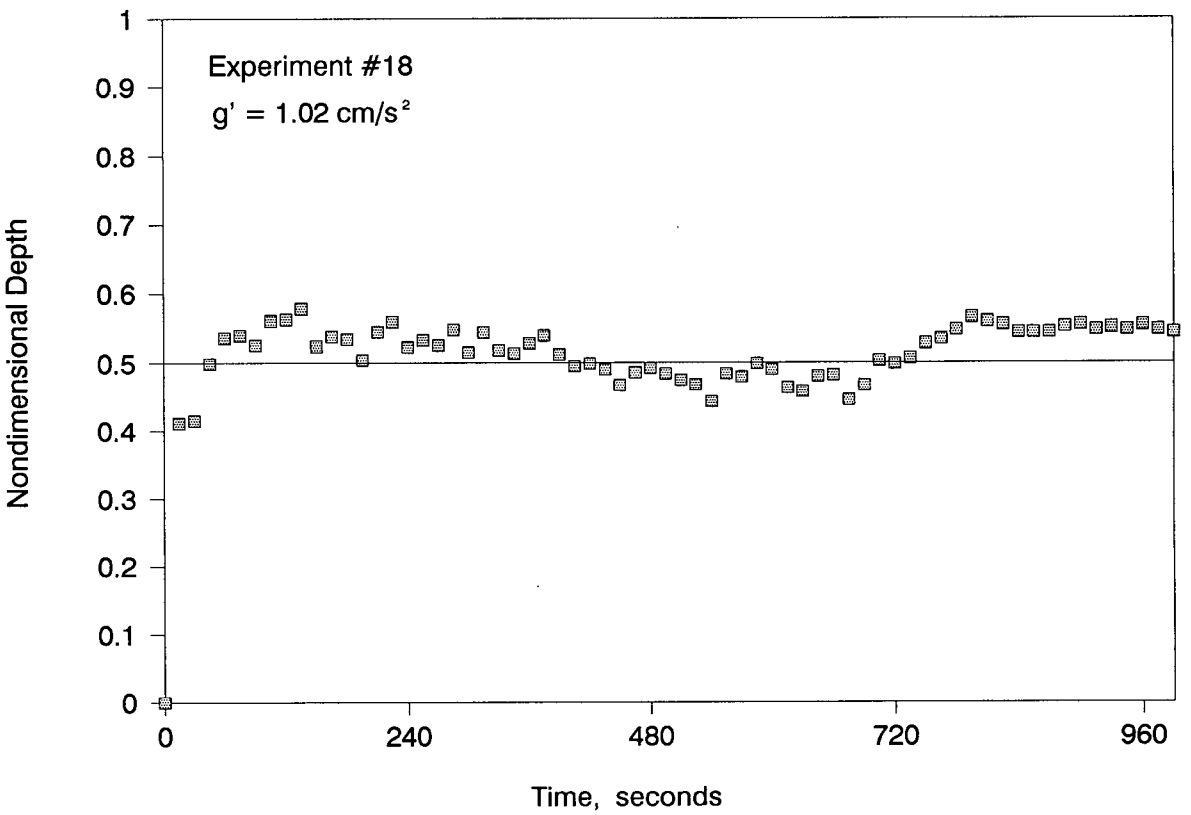

Figure 16. Long term variation of the interface height at the throat for Experiment #18

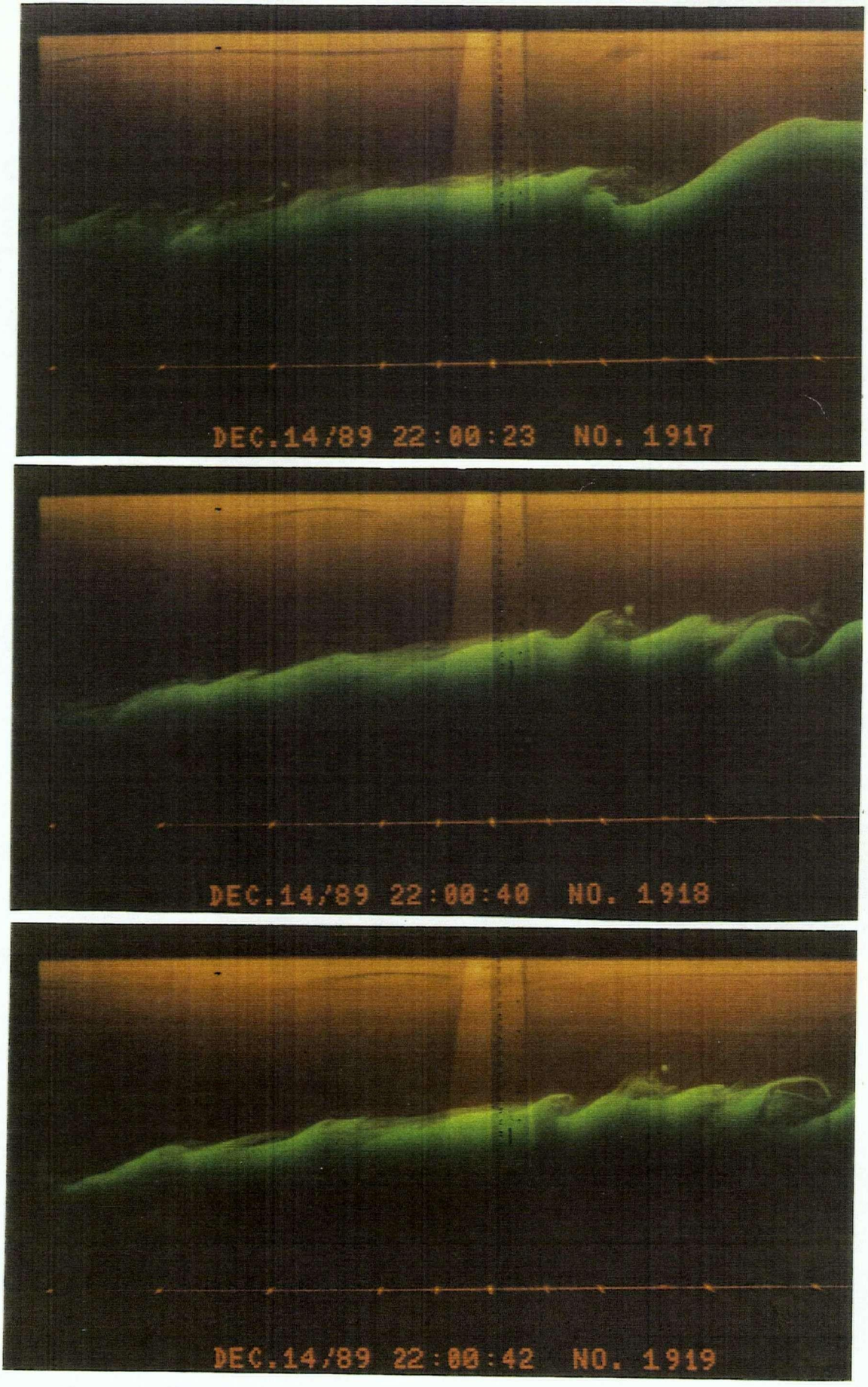

Figure 17. Sequence of photographs showing Kelvin-Helmholtz instabilities from Experiment #19

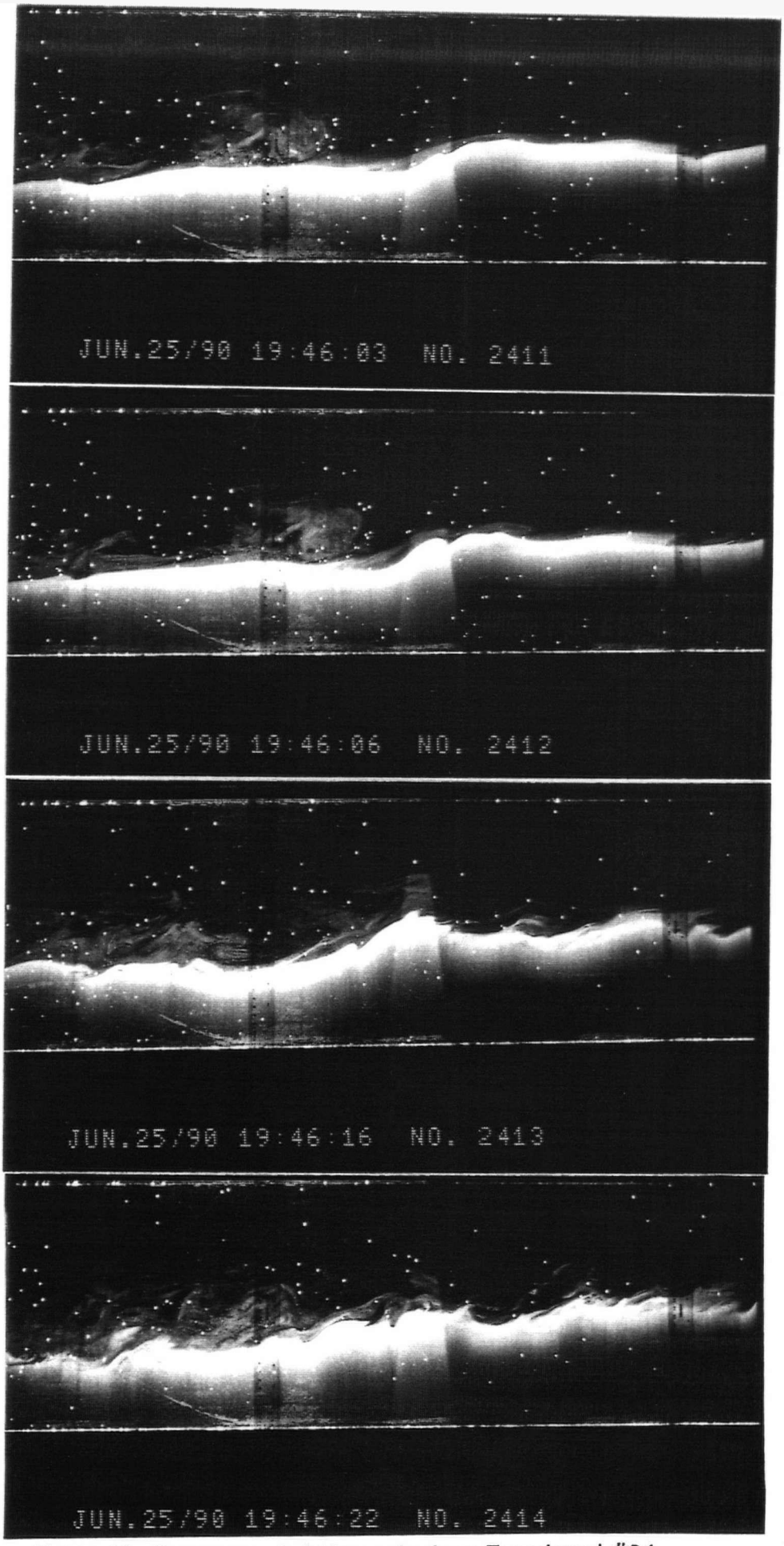

Figure 18. Sequence of photographs from Experiment #24

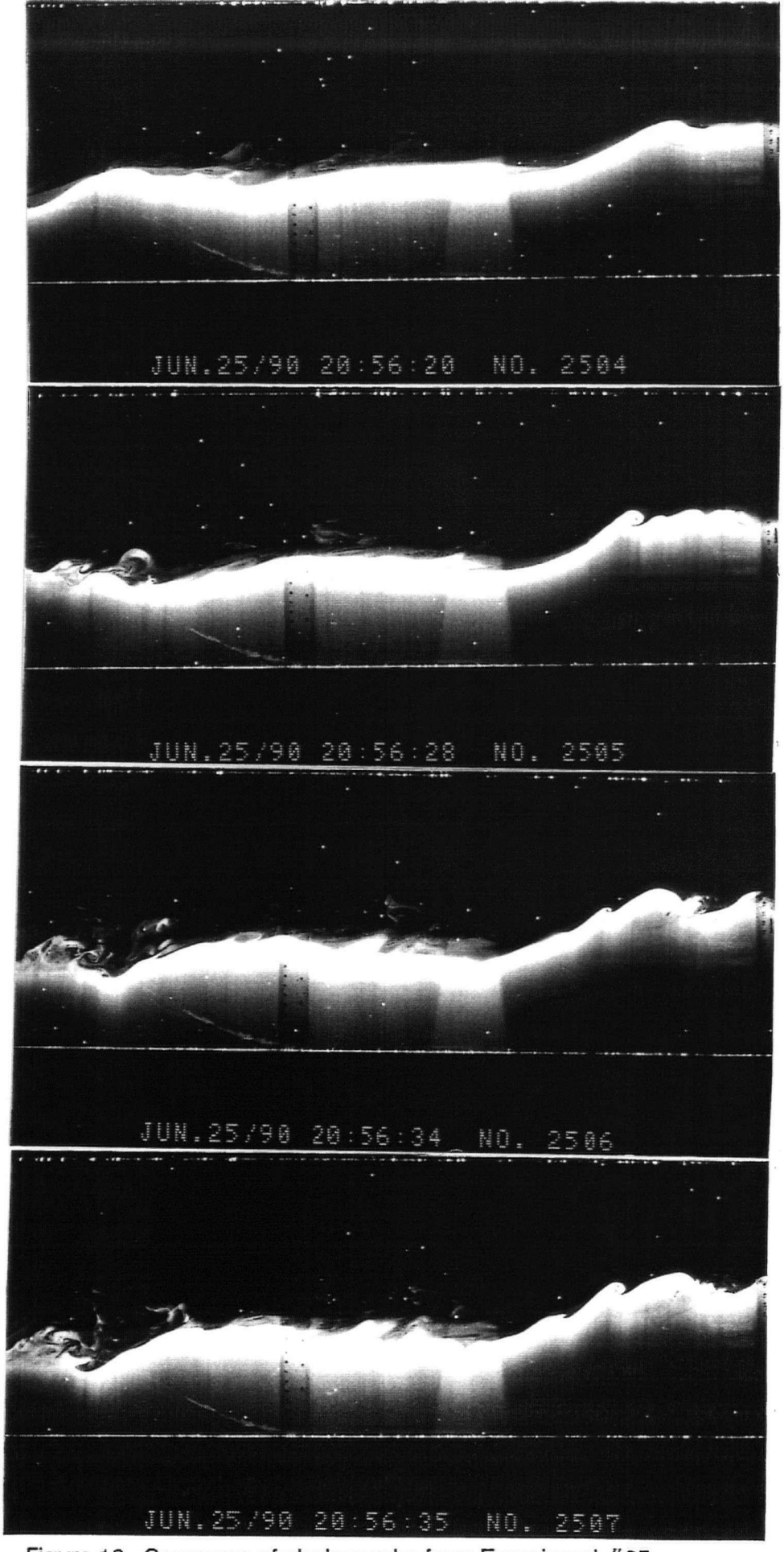

Figure 19. Sequence of photographs from Experiment #25

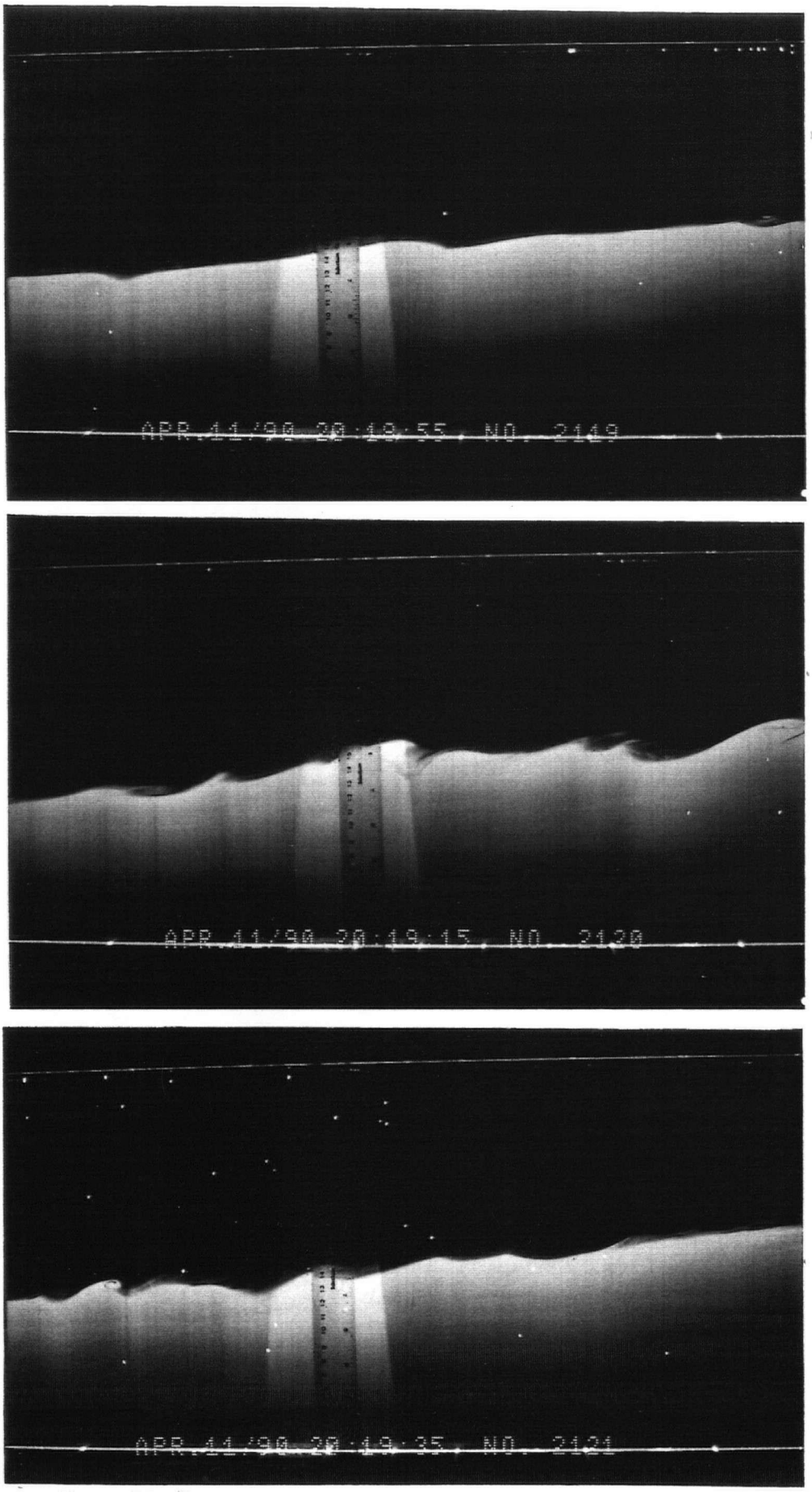

Figure 20. Sequence of photographs with Kelvin-Helmholtz and Holmboe instabilities from Experiment #21

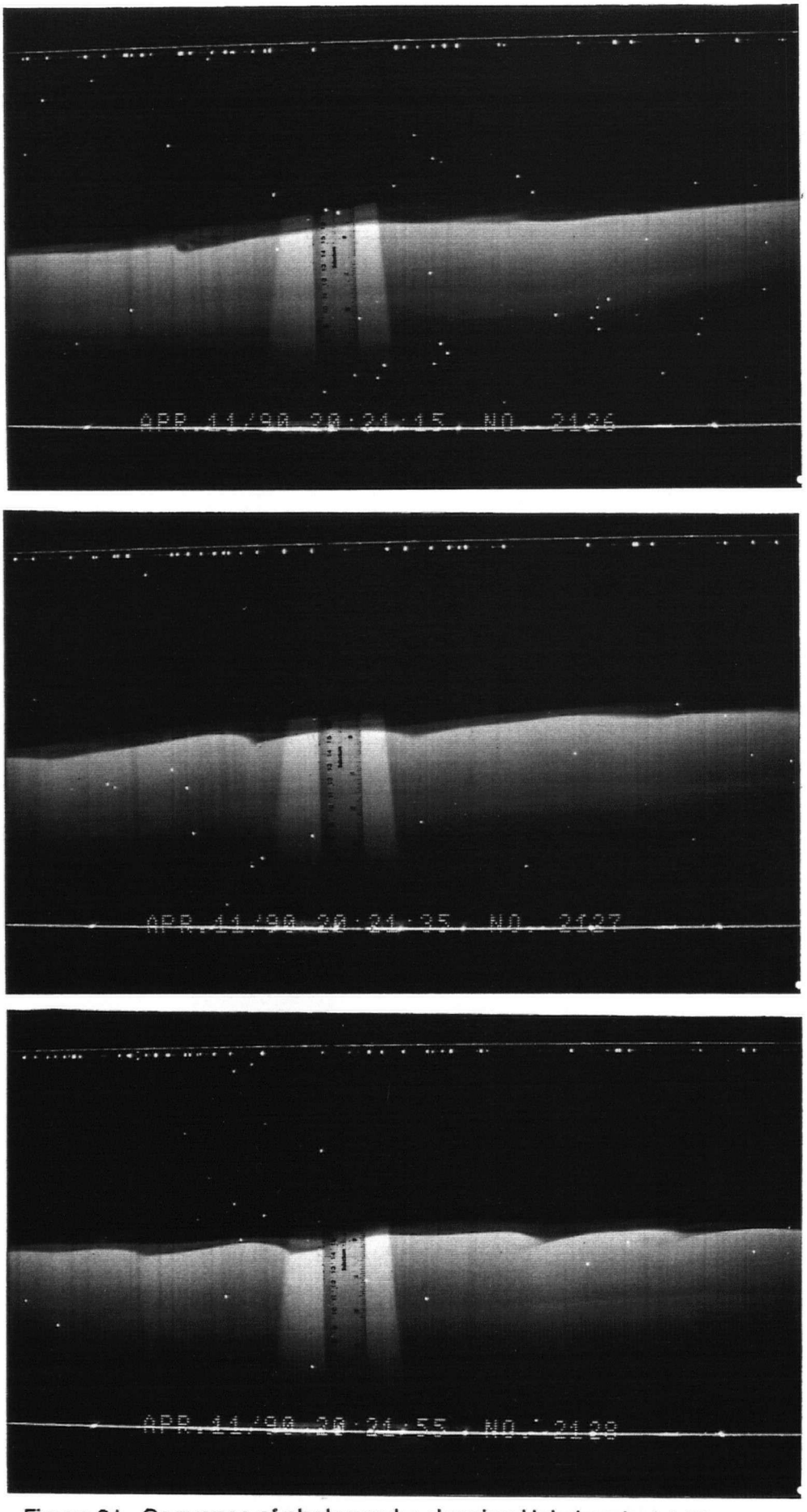

Figure 21. Sequence of photographs showing Holmboe instabilities

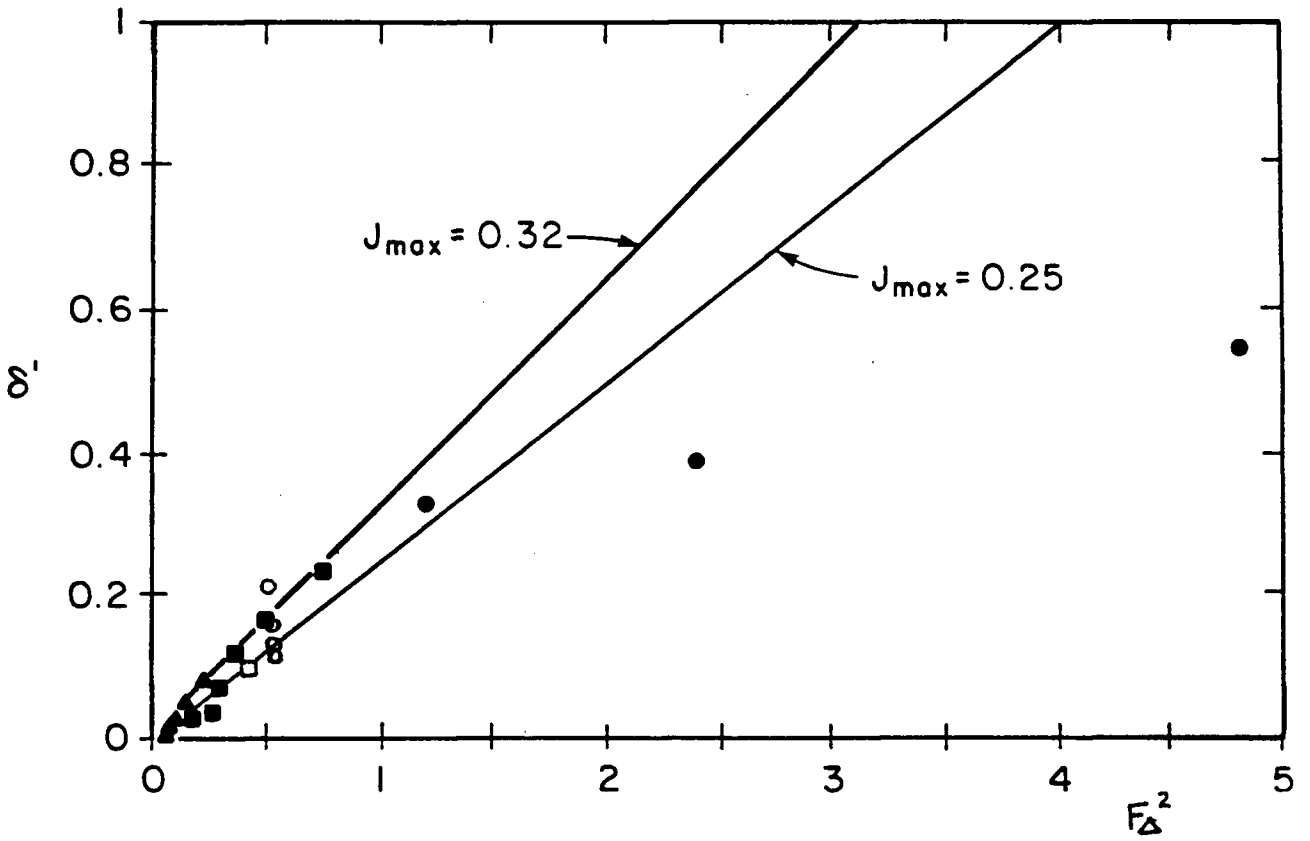

Figure 22. Variation of dimensionless maximum interface thickness with the stability Froude number

- ■ Koop and Browand (1979)
- □ Lawrence (1985)
- ▲ Lawrence, Browand & Redekopp (1990)
- ● Lawrence, Guez & Browand (unpublished)
- o Cheung

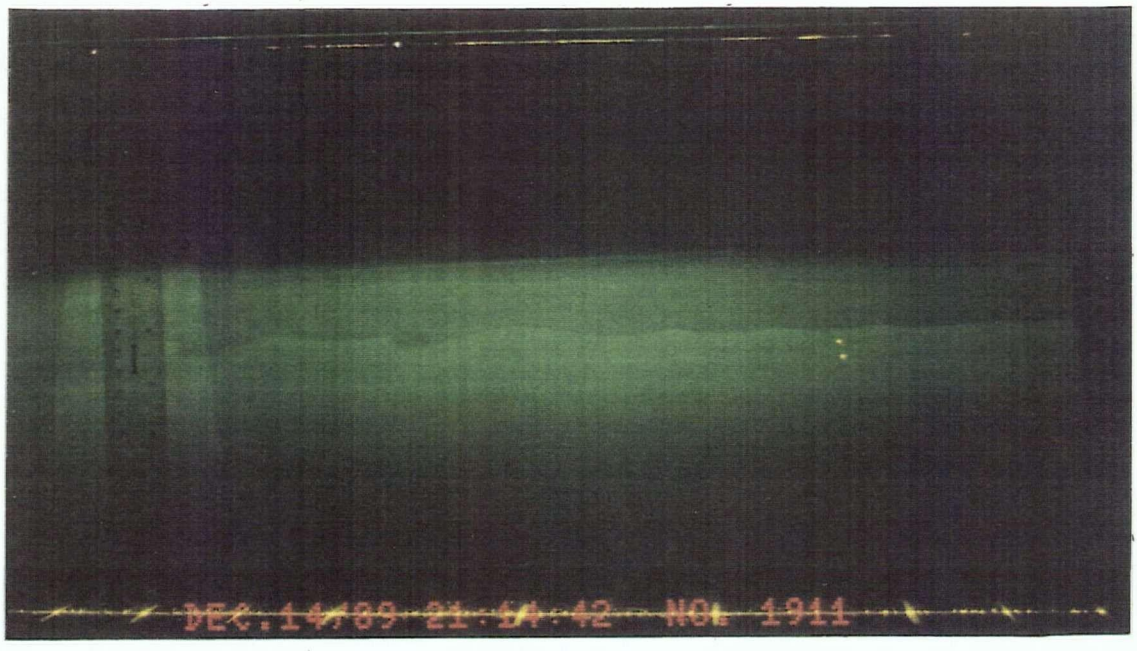

Figure 23. Photograph of the interface thickness

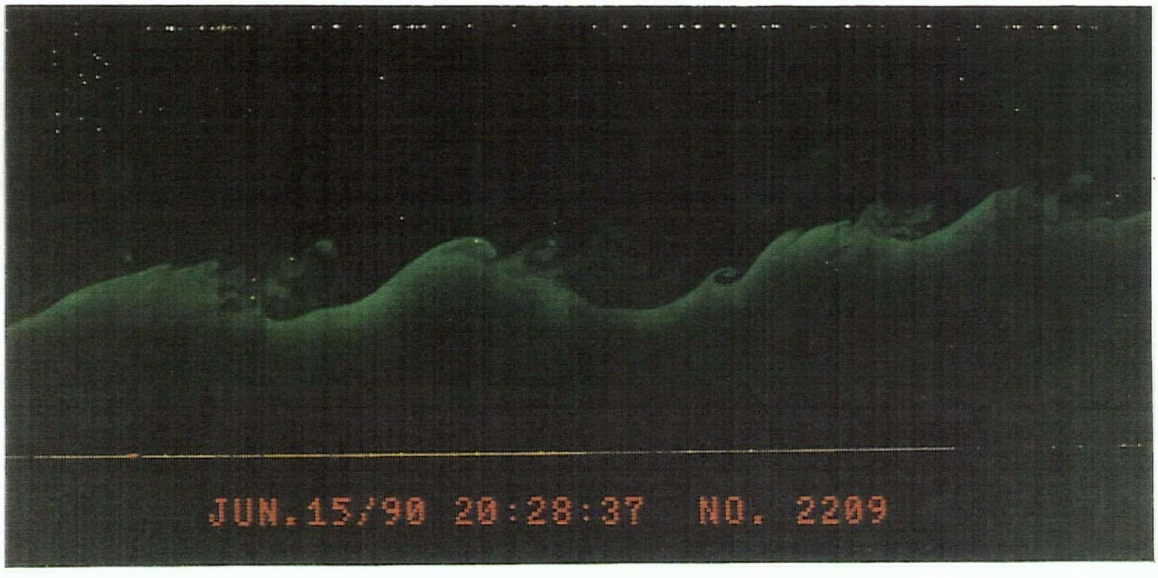

Figure 24. Photograph of wavelengths of the Kelvin-Helmholtz mode

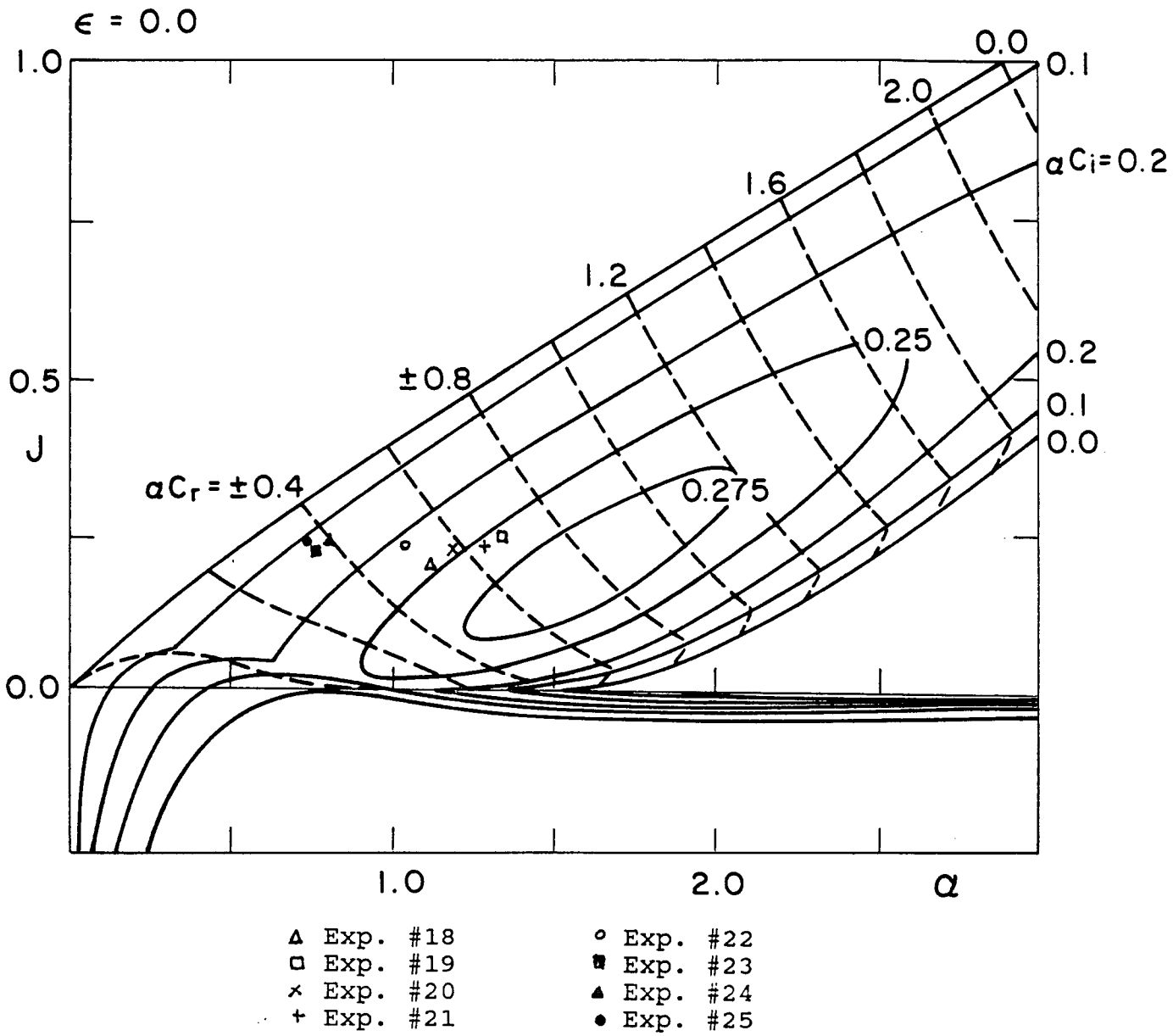

Figure 25. Stability Diagram (Lawrence et al. 1990)

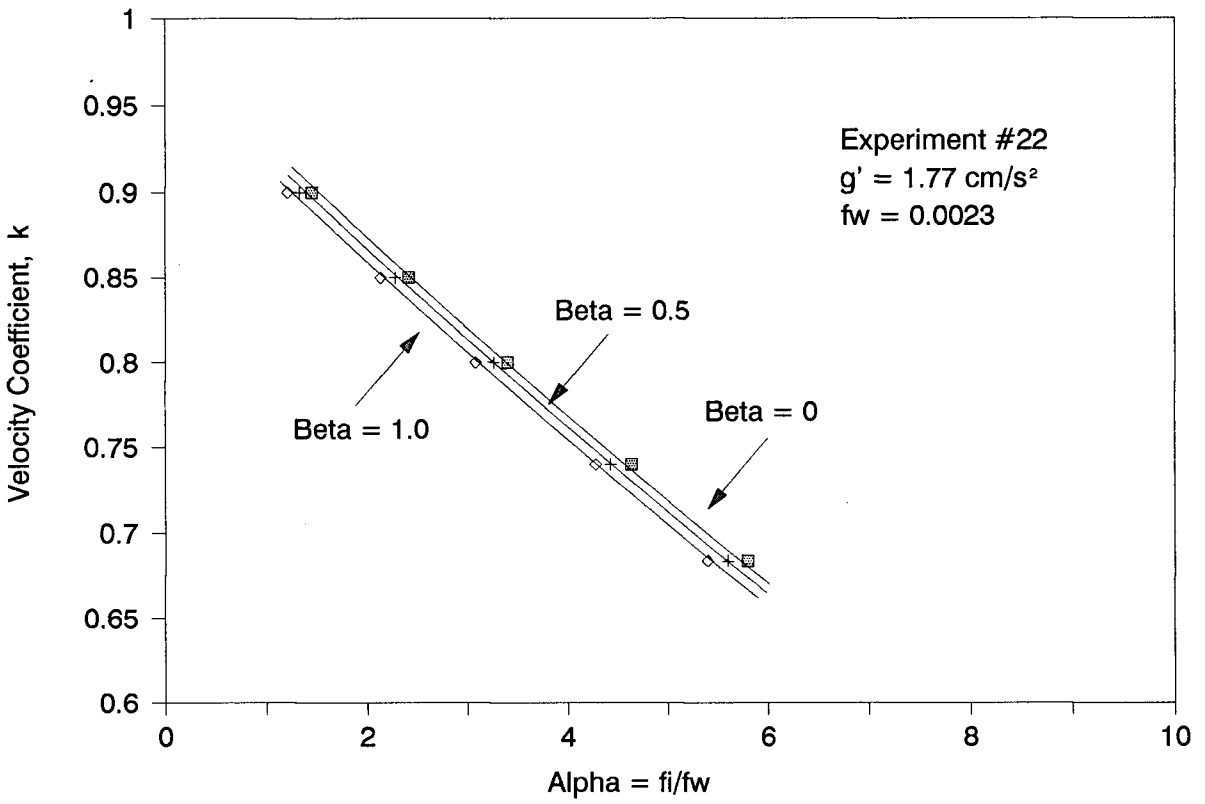

Figure 26. Variation of calculated k and alpha with beta = 0, 0.5, and 1.0

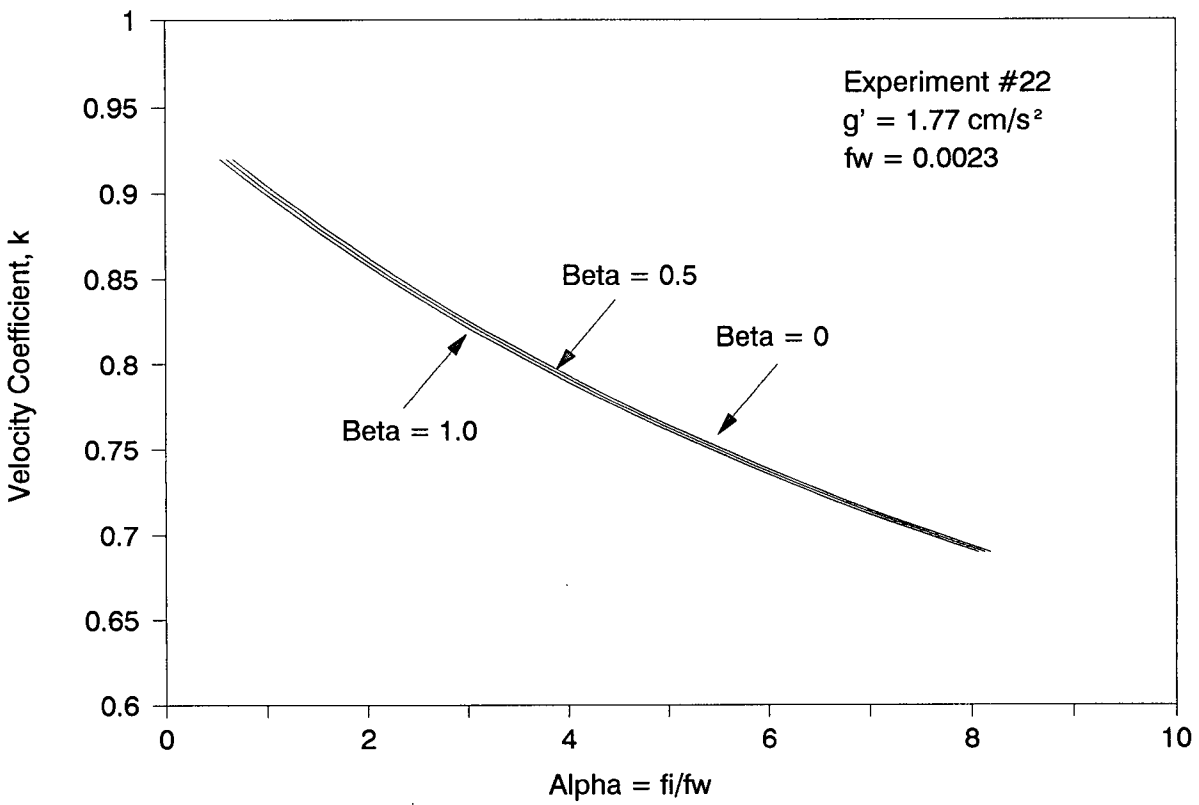

Figure 27. Theoretical variation of k and alpha with beta = 0, 0.5, 1.0

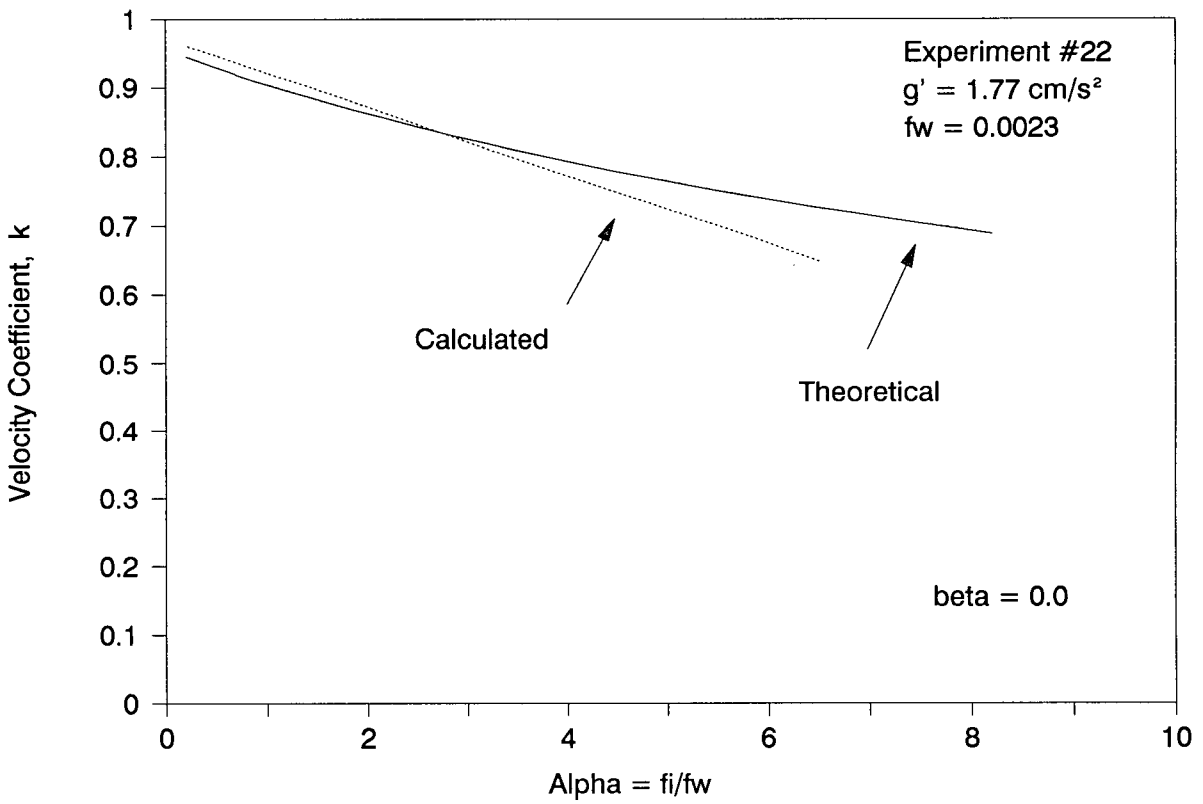

Figure 28. Comparison of theoretical and calculated curves of k and alpha for beta = 0

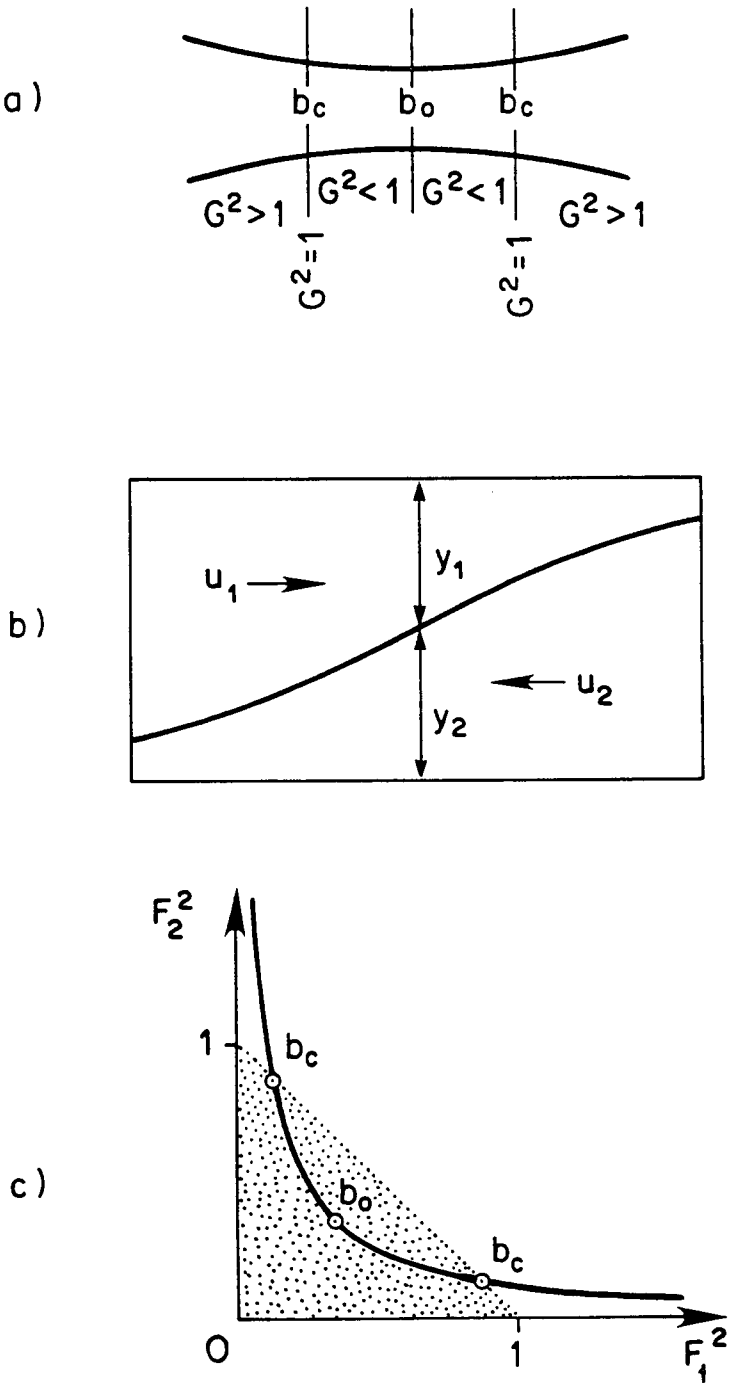

Figure 29. Variation of: a)the composite Froude number through a contraction, b)interface height along a section of a contracted channel, c)the Froude numbers for each layer shown on a Froude number plane